



UNIVERSITY OF NAIROBI

**A STUDY OF HYDROXYL (OH) MASER
VARIABILITY IN NGC 6334I**

BY

PETER JAIROUS BANDA

I56/89604/2016

**A Thesis Submitted in Fulfillment of the Requirements for Award of the Degree of
Master of Science in Physics of the University of Nairobi**

2019

DECLARATION

I declare that this thesis is my original work and has not been submitted elsewhere for examination, award of a degree or publication. Where other people's work or my own work has been used, this has properly been acknowledged and referenced in accordance with the University of Nairobi's requirements.

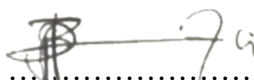
Peter Jairous Banda

I56/89604/2016

Department of Physics

School of Physical Sciences

University of Nairobi


Signature 

Date 12/03/2019

The undersigned have agreed to supervise the proposed research leading to the award of a MSc degree in Physics from the University of Nairobi.

Signature

Date

Dr. Geoffrey O. Okeng'o 

12/03/2019

University of Nairobi

Department of Physics

P. O Box 30197-00100, GPO, Nairobi-Kenya.

Email: geffok@gmail.com

Dr. Gordon C. MacLeod 

Type text here

12/03/2019

Hartebeesthoek Radio Astronomy Observatory

P. O Box 443, Krugersdorp 1740, South Africa

Email: gord@hartrao.ac.za

ABSTRACT

The Cat's Paw Nebula is part of our host Milky Way galaxy which experienced a significant assumed accretion event resulting in highly variable hydroxyl, water and methanol masers. Not only were these masers variable in intensity but also velocity. The source NGC 6334I was included on the long-term observational program at Hartebeesthoek Radio Astronomy Observatory and we report some of the findings.

We find that the peak velocity of some OH maser features varied periodically and experienced a maximum velocity variance of about 8 –10 %. The variance was observed in both the LCP and RCP of the OH maser dynamic spectra. In LCP, the variation was observed at -10.6 km s^{-1} , and -10.2 km s^{-1} and the period of variability was 366.01 ± 3.33 and 365.89 ± 1.28 days respectively. In RCP, the velocity only varied periodically at -6.7 km s^{-1} and its period was found to be 366.69 ± 1.38 days. The period is within the error of one Earth year (365 days).

A source identified as NGC 6334-V south of NGC6334I, which is not at the beam center of the telescope, has 1665 MHz OH masers that were detected while observing those from NGC 6334I. As a result of its large angular distance from the beam center (NGC 6334I), the applied local standard of rest velocity (V_{lsr}) correction introduced a periodic variation for OH masers originating from NGC 6334-V. Masers from this source whose Earth-Sun motion was not corrected are roughly at angular separation of $50'$ corresponding to the velocity of -10.2 km/s , $42.5'$ corresponding to the velocity of -6.7 km s^{-1} and $40'$ corresponding to the velocity of -10.6 km s^{-1} .

We attempted to determine the magnetic field strength by firstly identifying Zeeman pairs based on the fact that they have similar variability. The magnetic field corresponding to 1665 MHz OH masers from NGC 6334I was found to be $-5.8 \pm 0.5 \text{ mG}$

The five years of data used for this study were provided by Hartebeesthoek Radio Astronomy Observatory (HartRAO) in South Africa. The data was processed and reduced using an in-house program called *lines* which run on Linux and the analysis was done using a program called *Period04* and also using python scripts in Jupyter Notebook. The period of variation was obtained by fitting a sine function to the observational data.

Contents

DECLARATION	ii
ABSTRACT	iii
LIST OF TABLES	vi
LIST OF FIGURES	viii
LIST OF ABBREVIATIONS	ix
1 CHAPTER ONE: INTRODUCTION	1
1.1 Astrophysical Masers	1
1.2 Background of Hydroxyl (OH) Masers	1
1.2.1 OH Masers in Star Forming Regions	2
1.2.2 The NGC 6334I - A Star-Forming region	2
1.3 Statement of the problem	3
1.4 Main Objective	4
1.4.1 Specific Objectives	4
1.5 Justification and Significance of the Study	4
2 CHAPTER TWO: LITERATURE REVIEW	6
2.1 Introduction	6
2.2 Hydroxyl (OH) Maser	6
2.3 Zeeman Effect And The Magnetic Field	8
3 CHAPTER THREE: THEORETICAL BACKGROUND	9
3.1 Introduction	9
3.2 OH Maser Transitions	9
3.3 Zeeman Effect	12
4 CHAPTER FOUR: MATERIALS AND METHODS	15
4.1 Introduction	15
4.2 Description and Characteristics of the Telescope	15
4.3 Observation Method.	16
4.4 Data Processing and Reduction.	17

4.5	Data Analysis	21
4.5.1	Pointing Check and Correction.	21
4.5.2	Determination of Period of Variability in Velocity.	24
4.5.3	Approximation of Angular Separation of Maser Sources Causing Peri- odic Variation	27
4.5.4	Removal of Infringing Masers From The Dynamic Spectra	27
4.5.5	Identification of Zeeman Pairs and Magnetic Field Calculation	28
5	CHAPTER FIVE: RESULTS AND DISCUSSION	29
5.1	Introduction	29
5.2	Variability in V_{lsr}	29
5.2.1	Approximation of Angular Distances Using Calculated V_{lsr}	30
5.2.2	Pointing Check results	31
5.2.3	Removal of Infringing Masers Results	36
5.3	Flaring of 1665 MHz OH Maser in NGC 6334I	37
5.4	Magnetic Field in NGC 6334I	41
6	CONCLUSION AND RECOMMENDATIONS	43
6.1	Conclusion	43
6.2	Recommendations	43
	APPENDIX A1	45
	APPENDIX A2	47
7	LIST OF REFERENCES	71

List of Tables

2	Observing parameters for the Hartebeesthoek 26 m radio telescope (source: www.hartrao.ac.za)	16
3	Results of period and amplitude calculations using period04 for the 1665 MHz OH maser associated with NGC 6334I obtained from observational data.	30
4	V_{lsr} correction values using period04 for the 1665 MHz OH maser associated with NGC 6334I	31
5	Pointing parameters and the associated errors conducted on 21 September 2017 for specific 1665 MHz OH maser velocities that showed periodic variation in the LCP	34

List of Figures

1	Image of NGC 6334 with all associated maser sources reported so far.	3
2	1665 MHz hydroxyl (OH) maser radiative pumping model in which masing occur between level 3 and level 1	10
3	(a): A model of hydroxyl molecule with the z-axis along the nuclear of the two atoms. (b): Ground state rotational ladder (${}^2\Pi_{3/2}$) of the OH molecule and its allowed energy transition. (source: De Buizer, 2002)	11
4	An image of the 26 m Hartebeesthoek radio telescope located in Krugersdorp, South Africa. (source: www.hartrao.ac.za)	15
4	Stages in the spectral line data processing and reduction of 1665 MHz OH masers using the <i>lines</i> program for the left and right circular polarization (LCP and RCP).	20
5	Images showing the telescope pointing scans for the source NGC 6334I for the cardinal points North-South, East-West and the center. Note that the band-pass and the baselines were not corrected yet for the above images	22
6	The pointing spectra for the North, South, East, West, and Central after band-pass response and residual baselines have been corrected and removed.	23
7	Dynamic spectra of the 1665 MHz OH maser showing the variation of velocity with time on the scale of days as obtained from each day of observation	25
8	Time series plots showing variation in velocity of the 1665 OH maser associated with NGC 6334I for both the LCP and RCP. In the RCP the OH maser varies periodically at about a velocity of -6.7 km s^{-1} while in the LCP the variation occurs at -10.2 km s^{-1} and -10.6 km s^{-1}	26
9	Plots (a), (b), and (c) are variations in the velocity of 1665 MHz OH maser observed towards NGC6334I	29
9	Light curves of V_{lsr} for the 1665 MHz OH maser calculated at varying distances from NGC6334I for each day of observation and fitted with a sine function.	33
10	Image showing continuum emission of multiple star-forming regions in NGC6334	35
11	Images showing the process of removing infringing masers in NGC 6334I.	36
12	image of time series showing the variation of flux with time in the LCP and RCP at various velocity channels	38
13	Zeeman pairs and magnetic field studies conducted by Fish <i>et al.</i> , 2003	68

14 Abstract of a paper that contain some of the results of this thesis which was published in 2018. This paper is available online. 69

15 Abstract of a paper that has been submitted for publication written by Banda *et al.*, 2018 70

LIST OF ABBREVIATIONS

2MASS	Two Micron All-Sky Survey
ATCA	Australia Telescope Compact Array
AVN	African VLBI Network
CO	Carbon Monoxide
C₂S	Carbon Sulphide
DEC	Declination
H I	Neutral Hydrogen atoms
H II	Ionized Hydrogen atoms
HartRAO	Hartebeesthoek Radio Astronomy Observatory
H₂CO	Formaldehyde
H₂O	Water Molecule
HEMT	High Electron Mobility Transfer
IR	Infrared
ISM	Interstellar Medium
JD	Julian Date
Jy	Jansky
LASER	Light Amplification by Stimulated Emission of Radiation
LCP	Left Circular Polarization
LPV	Long Period Variable stars
L_☉	Solar Luminosity
M_☉	Solar Mass
MASER	Microwave Amplification by Stimulated Emission of Radiation
MERLIN	Multi-Element Radio Linked Interferometer Network
MJD	Modified Julian Date
NGC	New General Catalogue
OH	Hydroxyl radical
pc	Parsec
PSS	Point Source Sensitivity
RA	Right Ascension
RCP	Right Circular Polarization
RFI	Radio Frequency Interference
rms	Root Mean Square

SEFD	System Equivalent Flux Density
VLA	Very Large Array
VLBI	Very Long Baseline Interferometry
V_{lsr}	Velocity Local Standard of Rest
UCHII	Ultra Compact H II

1 CHAPTER ONE: INTRODUCTION

1.1 Astrophysical Masers

MASER is a short form for *Microwave Amplification by Stimulated Emission of Radiation*. Astrophysical masers are therefore stimulated spectral line emission that occur naturally in the microwave region of the electromagnetic spectrum. The sources of astrophysical masers include molecular clouds, comets, planetary atmospheres and atmospheres where active star formation is taking place (Elitzur *et al.*, 1992). Different molecular species such as Hydroxyl (OH), Water (H₂O), Methanol (CH₃OH) and many others have been observed in these regions using radio telescopes such as the 26 m telescope at Hartebeesthoek Radio Astronomy Observatory in South Africa.

Masers from molecular clouds and star forming environments are highly variable. Maser variability generally refer to the change in brightness (flux density), width and the velocity to the observer. Variations in the brightness can occur on the timescale of days to years (Gray, 2012). This work focused on studying the variability of 1665 MHz OH masers originating from an active massive star forming region known as NGC 6334I found in the Cat's Paw Nebula.

Astrophysical masers are very important in the study of star-forming regions because, they are able to penetrate the most obscured regions of molecular clouds allowing us to have an understanding of the physics that occur in these regions (Gray, 2012).

1.2 Background of Hydroxyl (OH) Masers

Since their discovery, astronomical *masers* have been used to study regions of star formation (Weaver *et al.*, 1965). The hydroxyl (OH) radical was first observed as an absorption line towards Cassiopeia A (Weinreb *et al.*, 1963). The same line was also observed in absorption at 1665 and 1667 MHz towards Sagittarius A (Robinson. 1964). Using a high-resolution spectrometer, the observed lines could be resolved and it was possible to distinguish between OH absorption and emission sources (Weaver *et al.*, 1965; Perkins *et al.*, 1966; Litvak *et al.*, 1966). Weaver *et al.*, (1965) suggested that the emission lines are the allowed ground-state maser transition of OH molecules which was confirmed by Weinreb *et al.*, (1965) who detected three OH transitions in the rotational ground state at the predicted molecular transition frequencies and established they were stimulated emission sources which were 37 percent linearly polarized. It was also found that OH maser sources and H II regions are associated

with young stellar objects which supply power for OH maser emission (Zuckerman *et al.*, 1965).

1.2.1 OH Masers in Star Forming Regions

It was found that 1665 MHz OH maser features were associated with star formation (Moran *et al.*, 1968) as a result they were described as sign-posts for star formation. The maser emission originates from the molecular envelope surrounding an ultra-compact H II (UCHII) region (Neugebauer and Leighton., 1997). It is referred to as interstellar masers, because the masers originate inside molecular clouds where stars form.

Past studies have shown three basic properties of masers. First, that maser spectral lines are much narrower and stronger as compared to those resulting from thermal emission. Second, maser sources usually have many individual masing regions each having a well-defined velocity and third, the regions from which masers originate have dimensions of the order 10^{13} cm in star-forming regions (Wright, 2001).

The OH masers are variable in regions of star formation and the causes of the variability are several. For instance, one cause of variation is intrinsic variation. This type of variation is as a result of maser responses to a series of pump disturbances or fluctuations of the masing level populations about their steady state (Clegg *et al.*, 1991). The pump disturbances are usually caused by shocks which may result from stellar winds, jets, rotating accretion disk and in-fall of inter-stellar material. The variations in maser sources would result in variation in the maser flux, line width and its radial velocities.

1.2.2 The NGC 6334I - A Star-Forming region

NGC 6334 is a large and complex massive star-forming region located in the Cat's Paw Nebula in our Milky Way galaxy. Contained in NGC6334 are multiple UCH II regions which also has an infrared/millimeter source called NGC 6334I-MM1 (Harvey and Gatley . 1982). Figure 1 shows an image of multiple maser centers of which from interferometric observations could be resolved into four continuum sources MM1-4 (Hunter *et al.*, 2006; Brogan *et al.*, 2016). This region was also found to contain three far-infrared sources which were identified as OH maser sources and two compact H II regions (Emerson *et al.*, 1970). Other studies of the region looking at carbon monoxide (CO) emission and formaldehyde (H_2CO)

absorption show that the whole cloud of NGC 6334 is collapsing with a velocity which is proportional to the radial distance from the center and that all sites of star formation are embedded within this single cloud (see e.g Dickel and Wilson. 1977). NGC 6334I is located at the coordinates Right Ascension (R. A) $17^h 20^m 53^s.4$ and Declination $-35^{\circ} 47' 1''$

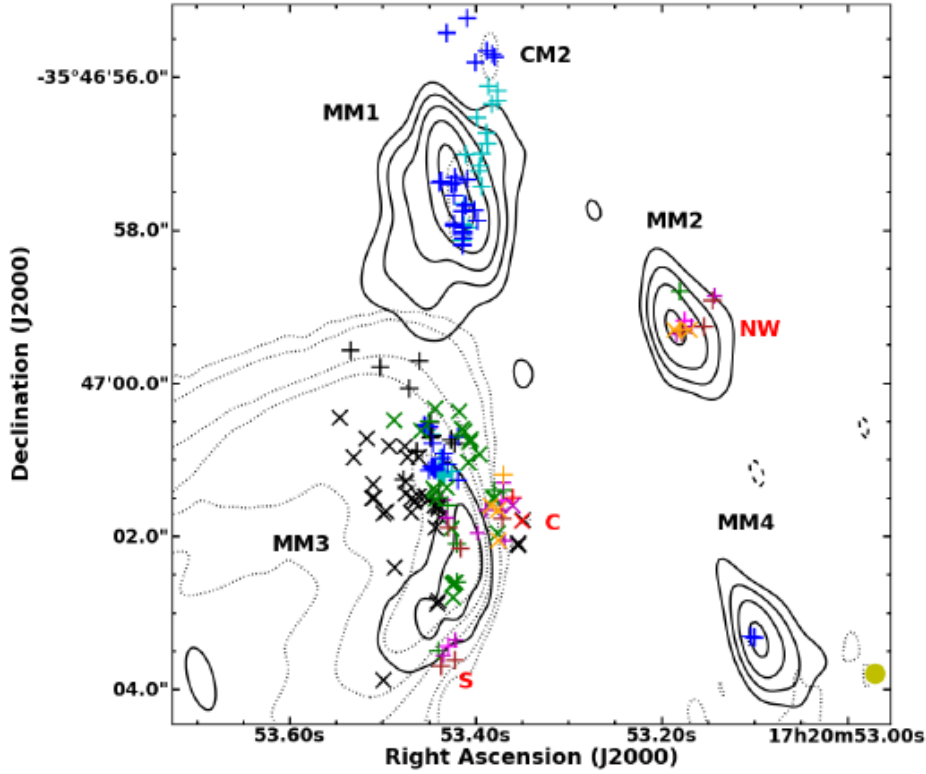


Figure 1: Image of NGC 6334 with all associated maser sources reported so far.

(Source: MacLeod *et al.*, 2018)

1.3 Statement of the problem

Systematic variation in the flux of the OH, methanol and water masers towards NGC 6334I were recently identified and reported by MacLeod *et al.*, 2018. The observed variation in 1665 MHz OH masers appear periodic in velocity in some features and the underlying cause of the periodicity are not well understood. This work investigated the periodic variation in three of the 1665 MHz maser velocity features and the cause of the variability was determined.

The source NGC 6334I has also been observed to show flaring in methanol and water (MacLeod *et al.*, 2018). A recent explanation by Hunter *et al.*, (2017) proposed that an accretion event had occurred providing the necessary energy for all the masers including

the OH features associated with this significant flare. Here the flaring event in the maser features showing periodic variation in peak velocity was further investigated. The relationship between maser variation and magnetic field strength in the star-forming regions remain unclear (Gerald *et al.*, 1990; Heiles *et al.*, 1993; Vlemmings *et al.*, 2005) and this work will attempt to determine the strength of the magnetic field by identifying 1665 MHz OH Zeeman pairs and also by looking at the similarity in the variation between LCP and RCP features.

1.4 Main Objective

The main objective of this work is to study the variability of 1665 MHz masers associated with NGC 6334I and determine the magnetic field strength.

1.4.1 Specific Objectives

The specific objectives of the study are:

1. To determine the period of variability in the velocity components of the 1665 MHz OH maser and the error associated with it.
2. To explore the cause of the periodic variations in the peak velocity and the flaring event and offer a possible explanation.
3. To identify Zeeman pairs and use them to determine the magnetic field strength of 1665 MHz OH maser features associated with NGC 6334I.

1.5 Justification and Significance of the Study

The periodic variation in velocity of 1665 MHz OH maser features remains a strange and interesting phenomenon that require proper investigation and understanding. In this work, the period of variation in the peak velocity was studied and the findings will greatly help in future observation of the source.

Since the region also exhibited epochs of flaring in maser features such as methanol, water and excited OH maser transitions, some flaring was also observed in 1665 MHz OH masers and periodic velocity variation will provide additional information relating to the region (MacLeod *et al.*, 2018; Hunter *et al.*, 2017). This phenomenon was investigated further and the knowledge acquired will contribute to understanding the dynamic nature of the star-forming region.

Furthermore, magnetic field strength plays a significant role in the splitting of energy levels of masing molecules in star-forming regions. Therefore, identification of the Zeeman pairs and hence determination of magnetic field strength surrounding star-forming regions have a direct implication in understanding the conditions that surround star-forming regions.

2 CHAPTER TWO: LITERATURE REVIEW

2.1 Introduction

From the time OH masers were discovered, several scholars have used them to probe deeply embedded and obscured regions of star formation. Through the studies done so far, a lot has been learned and a lot still remain to be learned. This section, therefore, covered what has been learned about OH masers in star forming regions.

2.2 Hydroxyl (OH) Maser

The OH molecule was the first to be discovered in space as an absorption line and it was later observed in emission but was not identified as a maser (Weaver et al., 1965). Perkins *et al.*, (1966) and Litvak *et al.*, (1966) were the first to propose that intense OH emission found observed were masers. Many observations by various studies have been done at 1665 MHz searching for OH masers in star-forming regions (see e.g. Turner., 1970, Reid and Moran, 1981, Argon *et al.*,2000). Among the notable observations that were conducted include VLBI (Very Long Baseline Interferometry) experiments using telescopes across United States of America which led to the discovery that the OH emission comes from many spots with sizes of a few milli-arcseconds and brightness temperature of up to 10^{12} K. Most of the OH maser emission observed towards galactic compact H II regions were associated with star formation and thus firmly established to be signposts of active star formation (Wilson and Barrett 1968). Hydroxyl maser emission was also observed towards a number of Infrared (IR) sources listed in the Two Micron All Sky Survey (2MASS) (Neugebauer and Leighton, 1969). Most of the OH/IR sources in the list are Long Period Variable stars (LPV); they are known to be evolved stars in their red giant phase of evolution. This has led to the conclusion that maser emission is associated with both early and late stages of stellar evolution.

For strong maser activity to occur in astronomical settings, it is required that the gas density be considerably higher (10^5 to 10^{11} cm^{-3}) than that found in giant molecular clouds which is 100 cm^{-3} on average (Wilson et al., 1997). Also, a very high luminous source greater than $10^4 L_{\odot}$ can supply the energy to pump the masers. In most cases, the OH masers associated with star-forming regions, newly formed O-type or forming B-type stars supply the pumping energy. As a result, OH molecules are most likely contained in the condensation of interstellar material in the neighborhood of these luminous proto-stars.

Turner (1970) developed a morphological way of classifying OH sources based on their spectral characteristics. He came up with two main classes of the sources namely type I and II. A type I source is one strongest in the main lines which is a transition from upper (F=1) to lower (F=1) corresponding to a frequency of 1665.402 MHz and also the transition from upper (F=2) to lower (F=2) corresponding to a frequency of 1667.359 MHz (see figure 2). Sources which are type I and are associated with star-forming regions are strongest in the 1665 MHz transition. On the other hand, type II sources are strongest in the satellite lines which are transitions from upper (F=1) to lower (F=2) and upper (F=2) to lower (F=1) at frequencies 1612.231 MHz and 1720.530 MHz respectively. Typical interstellar hydroxyl (OH) maser spectra appear to consist many spectral components that span a range of about 10 km s^{-1} in radial velocity. The OH spectral components are circularly polarized up to 100 percent (Moran, 1976).

Compact H II regions (less than 1 pc in diameter) are usually found at nearly the same position as OH maser (Mezger et al., 1967). In almost all cases where the accuracy is better than $1''$, OH and radio continuum maps exist. These maps show that the masers project onto regions of H II emission. This leads to the conclusion that OH masers are physically associated with very young hot stars which create compact H II regions. Studies indicate that maser components normally cluster together on a scale size of 10^{12} km. On the other hand, Habing et al., (1974) noted that masers of more than 3×10^{14} km in extent do not have H II regions associated with them.

The first variability study of OH masers suggested changes in the flux of about 10 % on time scales of years (Sullivan *et al.*, 1976). Other studies of OH maser variability have indicated that flaring events sometimes occur periodically (Colom *et al.*, 2015). Another maser variability was reported in the 1667 MHz OH maser observed towards IRAS 16333-4807 and suggested that the stronger masers observed could have been due to shock excitation which resulted in the epochs (Qiao *et al.*, 2016). The most recent flaring was observed by MacLeod *et al.*, (2018) and Hunter *et al.*, (2017) in the methanol, water and OH masers towards NGC 6334I. Here we present detailed analysis of the 1665 MHz OH features in MacLeod *et al.*, (2018) where periodic velocity variations were detected.

Using 1.3 mm continuum emission, Hunter *et al.*, (2006) resolved NGC 6334I into four of which two are bright sources namely I-SMA 1 and I-SMA 2 which are presently identified as MM1 and MM2 respectively (see figure 1). The other centers associated with NGC 6334I are I-SMA 3 which also referred to as NGC 6334F and I-SMA 4- a new object recently discovered. In figure 1, I-SMA 3 corresponds to MM3 and I-SMA 4 corresponds to MM4. Hunter

et al., (2017) also reported an increase in dust temperature by a factor of 4.0 ± 0.3 in NGC 6334I. Each of the compact regions MM1-4 has associated interstellar material with masses ranging between 3 and $66M_{\odot}$.

2.3 Zeeman Effect And The Magnetic Field

When molecules are exposed to a magnetic field, the energy levels are slightly shifted from their normal state. This effect is known as the Zeeman effect or Zeeman splitting. The Zeeman effect is easily observed when masers produced by molecules in the magnetic field are circularly polarized (Crutcher *et al.*, 1990). Heiles (1993), identified the two methods for determining the Zeeman effect namely direct and indirect. The direct method involves identification of Zeeman pairs in linear and circular polarized masers while the indirect method involves the measurement of ambipolar diffusion of H_2O masers. Zeeman effect in OH masers can easily be determined by the direct method because they exhibit high circular polarization. The splitting is usually very small, however, the Zeeman effect and hence the magnetic field can still be estimated by subtracting the left circular polarization (LCP) from the right circular polarization (RCP).

By 1990, the Zeeman effect measured in space was from four species which included HI, OH, C_2S and H_2O and it was reported that the magnetic field ranged between a few micro Gauss (μG) in HI to about over $40\mu\text{G}$ in H_2O masers (Guisten *et al.*, 1990). Because of the large Zeeman effect and the ease with which it can be determined, OH masers have been extensively used to measure the magnetic field strength in massive star regions. Fish *et al.*, (2006) observed that the Zeeman effect is easily identified with high-resolution telescopes or VLBI. He also noted that OH masers can be used to measure the magnetic field strength because of its large Zeeman effect.

Colom *et al.*, (2015) did report findings of long-term monitoring of IRAS 20126+4104 from which periodic variability was noticed in the OH masers and also measured the Zeeman effect and hence found the magnetic field for two epochs (2008 and 2014) to be 1.3 mG and 10 mG respectively. Also, Qiao *et al.*, (2016) reported that the OH masers exhibited Zeeman effect for two events for which the magnetic field strength was determined as 2 to 10 mG observed towards IRAS 16333-4807 and suggested that OH maser emissions are born in the magnetic environment. As a result, we will attempt to identify the Zeeman pairs and hence the magnetic field strength of 1665 MHz OH masers towards NGC 6334I.

3 CHAPTER THREE: THEORETICAL BACKGROUND

3.1 Introduction

This chapter explains the physics behind the production of masers in molecules with a focus on the Hydroxyl (OH) molecule. Also explained theoretically is the Zeeman effect and how the Zeeman pairs can be used to calculate the magnetic field strength in star forming regions.

3.2 OH Maser Transitions

The physics behind microwave amplification (masers) in the interstellar medium (ISM) is similar to that behind light amplification (lasers). Molecules usually exist in their lowest energy states called the ground state. When molecules are exposed to radiation with energy, equal to the energy difference between the electronic energy states, the molecule will absorb the photon and excite the electron to the higher (excited) energy state. Since molecules in the ground state absorb energy in order to achieve excitation, the absorption coefficient K_ν of the molecules is given by the relation:

$$K_\nu = \frac{N_i h \nu B_{ij}}{\rho} \left(1 - \frac{g_i N_j}{g_j N_i}\right) \quad (1)$$

Where, N_i is the number of molecules in the lower energy state while N_j is that in the upper energy state, h is the Planck's constant, ν is the frequency of the incident radiation, ρ is the radiation flux, B_{ij} is the Einstein coefficient for the upward transition from low energy state to upper energy state while g_i and g_j are Lande factors (Elitzur, 1992).

Microwave amplification will only occur if the absorption coefficient has a value which is negative. This means that the number of molecules in the higher energy states are more than those in the lower energy state. This process of supplying energy to molecules in lower energy level in order to raise them to higher energy level is called pumping. The pumping process causes the number density of electrons in the higher energy level to be more than the number of electrons in the ground level, this state is called population inversion (Wright, 2001).

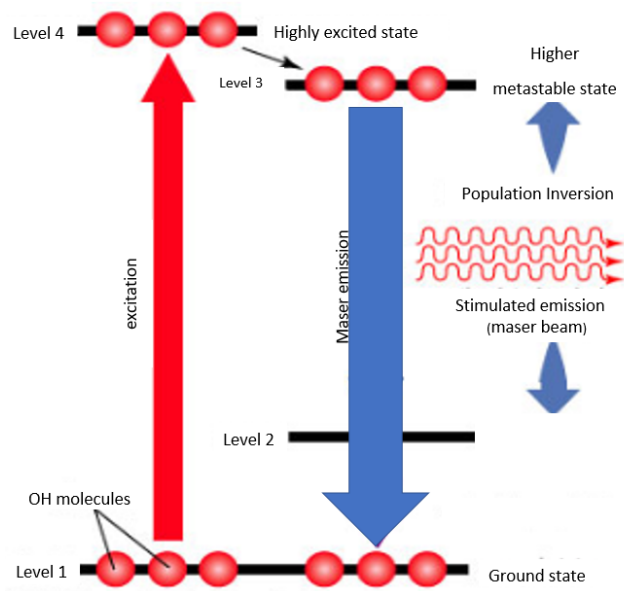


Figure 2: 1665 MHz hydroxyl (OH) maser radiative pumping model in which masing occur between level 3 and level 1

If the electrons fall from the higher energy level to the lower energy level on their own, they emit radiation which is called spontaneous emission. This type of emission is random, incoherent and generally does not result in amplification. However, if the fall is caused by an incident photon, stimulated emission takes place (see figure 2). This emission has the same phase and frequency as that of the incident photon (coherent) which causes them to additively increase resulting in an increased output energy. If this happens to many molecules in an excited state, the output is strongly amplified radiation. When this amplification occurs within the microwave region in the electromagnetic spectrum, the output radiation is called a maser.

In most cases, maser action occurs naturally in space when incident radiation traverses through a medium that has achieved a state of population inversion. The factor by which the maser is amplified is called the gain and it increases with an increase in column density of the active medium.

In star-forming regions, the column densities are usually very small. This is usually compensated by a long path length of the maser medium that are not doppler shifted out of its line-width. If the maser line-width of molecules in star-forming clouds are large, the lines will exhibit motion which varies internally due to spatial variation (Argon *et al.*, 2000). Therefore, to achieve a large gain, the maser photon must traverse through the star-forming cloud along good line of sight (one that is not Doppler shifted) and must exhibit velocity

coherence.

The OH radical is among the commonly observed molecules in star-forming regions and its molecular properties are hence discussed. It has a total angular momentum J given by:

$$J = L + S \quad (2)$$

where L and S is orbital angular and the spin momentum respectively. While in the ground state, the orbital angular momentum of the molecule is 1 and its projection on the z -direction (that is along its internuclear axis, see figure 3 a) is, therefore, $L_z = 1$. The z -direction spin components are $S_z = +\frac{1}{2}$ for spin up and $S_z = -\frac{1}{2}$ for spin down. Therefore, the total angular momentum in the z -direction can be written as $J_z = 1 + \frac{1}{2}$ or $J_z = 1 - \frac{1}{2}$. These are the two rotational ladders for the ground state with energies very close to each other when approximated to the first order. In other words, each value of orbital angular momentum is doubly degenerate, which means that for the ground state, $-J_z$ and $+J_z$, each has two accessible states giving a total of four accessible states (De Buizer, 2000).

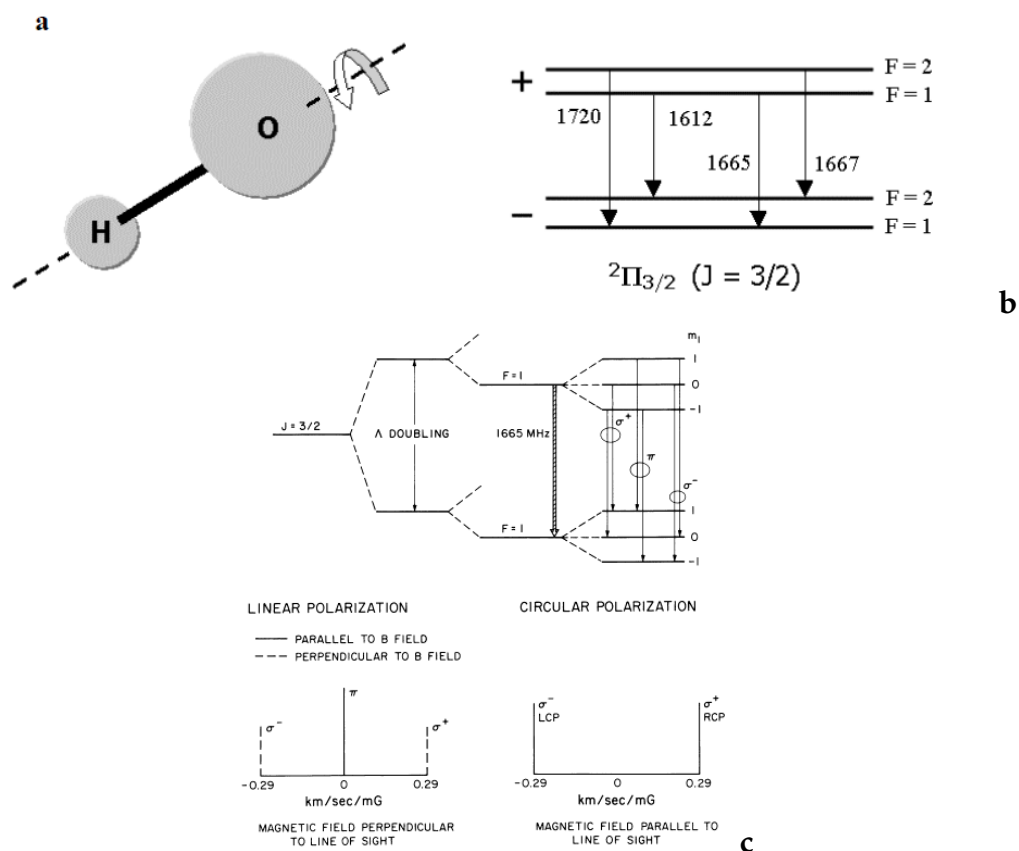


Figure 3: (a): A model of hydroxyl molecule with the z -axis along the nuclear of the two atoms. (b): Ground state rotational ladder ($^2\Pi_{3/2}$) of the OH molecule and its allowed energy transition. (source: De Buizer, 2002)

The energy difference between $+J_z$ and $-J_z$ are created by interactions between the orbital angular momentum (\mathbf{L}) and the nuclear rotation (\mathbf{I}). The spin due to the nuclear adds as a vector to the total angular momentum to give the final total angular momentum \mathbf{F} which is given by an expression

$$\mathbf{F}=\mathbf{J}+\mathbf{I} \quad (3)$$

This creates very weak splitting caused by the magnetic effect resulting from the nuclear spin. For a molecule having two atoms such as OH, its nuclear spin are $I_z = +\frac{1}{2}$ and $I_z = -\frac{1}{2}$ which results in the final total angular momentum in the z-direction equal to $F_z=2$, $F_z=1$ and $F_z=0$. Therefore, each state of the OH radical is split into four levels (See figure 3 b). This results into four allowed transitions with two main lines having the transition $\Delta F=0$, and the other two satellite lines having transitions $\Delta F=1$ and $\Delta F=-1$. Hence, for the ground state rotational ladder ${}^2\Pi_{\frac{3}{2}}$ ($J = \frac{3}{2}$) of OH (Wright, 2001), we obtain four spectral lines of which the two main lines with $\Delta F=0$ and the other two satellite lines with transitions $\Delta F=+1$ and $\Delta F=-1$. It should be noted that the transition from $\mathbf{F}=0$ to $\mathbf{F}=0$ is not allowed.

The most observed OH radical transitions by astronomers are the following frequencies 1667 MHz, a transition from upper ($\mathbf{F}=2$) to lower ($\mathbf{F}=2$) and 1665 MHz from upper ($\mathbf{F}=1$) to lower ($\mathbf{F}=1$). These form the main lines. However, the satellite lines are observed at 1720 MHz which is a transition from upper ($\mathbf{F}=2$) to lower ($\mathbf{F}=1$) and 1612 MHz transition from upper ($\mathbf{F}=1$) to lower ($\mathbf{F}=2$). In this research work, the main line of the OH maser transition at 1665 MHz was observed using the 26 m radio telescope at Hartebeesthoek Radio Astronomy Observatory (HartRAO).

3.3 Zeeman Effect

Molecules in a masing gas cloud will experience the Zeeman effect when in the presence of an external magnetic field. The strength of the Zeeman effect is dependent upon the field and magnetic susceptibility of the molecule. For the OH molecules, the energy levels are degenerate and when found in the presence of magnetic field, the degeneracy is split into hyperfine levels. Any given hyperfine transition results in two or more spectral lines with different polarization properties (Caswell *et al.*, 2011).

Hydroxyl masers often display pairs of strong left and right circularly polarized σ -components (see figure 3 C). For reasons that are not well understood, pure linearly polarized π -components are rare, if ever, detected. The task of identifying Zeeman pairs- two oppositely circularly

polarized lines at the same position on the sky is relatively simple provided one has sufficient angular resolution to resolve maser clusters (Fish & Reid, 2006). However, with VLA one can only achieve an angular resolution of about 1 arcsec for the OH transitions at 18 cm wavelength. If the emission in a spectral channel was to come from one unresolved spot on the sky, it would not be a significant limitation. Because, in reality, the emission in any given spectral channel can come from blends of masers at different positions in the source separated by less than the beam size.

Radiation emitted from energy levels of masing molecules created by the Zeeman effect emerge as either circularly or linearly polarized (see figure 3(c)). The measure of the splitting is directly related to the magnetic field strength.

$$\Delta v_z = \frac{g\mu_0}{\hbar} \mathbf{B} = b\mathbf{B} \quad (4)$$

where g is the Lande g factor, μ_0 is the Bohr magneton, b is a constant and B is the magnetic field (Crutcher *et al.*, 1990). Lande g factor and the Bohr magneton are given by:

$$\mu_0 = \frac{e\hbar}{2m} \quad (5)$$

$$g = 1 + \frac{j(j+1) + s(s+1) - l(l+1)}{2j(j+1)} \quad (6)$$

The polarization is unaffected during maser amplification if the Zeeman effect is small (Moriarty, 2009).

The Zeeman effect can easily be observed in circularly polarized emission. This is because the magnetic field present in a gas where spectral emission of an atom or molecule occur will cause the two senses to interact and hence cause circularly polarized components to split up in frequency (Wright, 2001). The degree of splitting of the LCP and RCP components vary directly with the strength of the magnetic field and a constant that is dependent on atomic or molecular transition, according to the relation:

$$\delta v = bB_{los}[mG](1+z)^{-1} \quad (7)$$

where, b is the Zeeman coefficient being observed and is measured in km s^{-1} per mili Gauss ($\text{km s}^{-1} \text{mG}^{-1}$), B_{los} is the magnetic field in the line of sight in miligauss (mG) and z is the redshift of source (Fish *et al.*, 2003).

The amplitude of Zeeman splitting is measured in the Stokes V spectrum and is defined by the relationship:

$$B[mG] = f(V_{RCP} - V_{LCP}) \quad (8)$$

where B is the magnetic field strength, V_{RCP} is the Stokes V spectrum for the right circular polarization and V_{LCP} is the Stokes V spectrum for the left circular polarization (Fish *et al.*, 2003).

For OH masers, amplitude measurements of Zeeman effect splitting towards sources in the galactic ISM are usually very weak when compared to the total intensity of the line measured in Stokes I spectrum. This is because, the splitting is very small compared to the line width (Davies, 1974). Magnetic field measurements in OH maser traces the large-scale uniform field in which the maser is embedded. The sign of the Zeeman splitting indicates the direction of the magnetic field as well as the magnitude which are mostly coherent (Fish *et al.*, 2003; Szymczak *et al.*, 2009).

Masers show the highest luminosity per unit frequency of any radio source, as a result, they are a natural choice to use this effect in regions of star formation to measure magnetic fields. Due to the large Zeeman coefficients of the various OH transitions, it can be used as a sensitive tracer of magnetic fields.

4 CHAPTER FOUR: MATERIALS AND METHODS

4.1 Introduction

In this chapter, the description of the telescope used to conduct the observations and how the data was processed before being analyzed are presented. Also present in this chapter is the detailed description of the methods used to analyze the data in-line with the study objectives.

4.2 Description and Characteristics of the Telescope

The observations of NGC 6334I were conducted using the 26 m radio telescope at Hartebeesthoek Radio Astronomy Observatory (HartRAO) in Krugersdorp near Johannesburg, South Africa (see figure 4). The dish is located at the coordinates; Latitude $25^{\circ} 53' 14''.4$ and Longitude $27^{\circ} 41' 05''.2$.

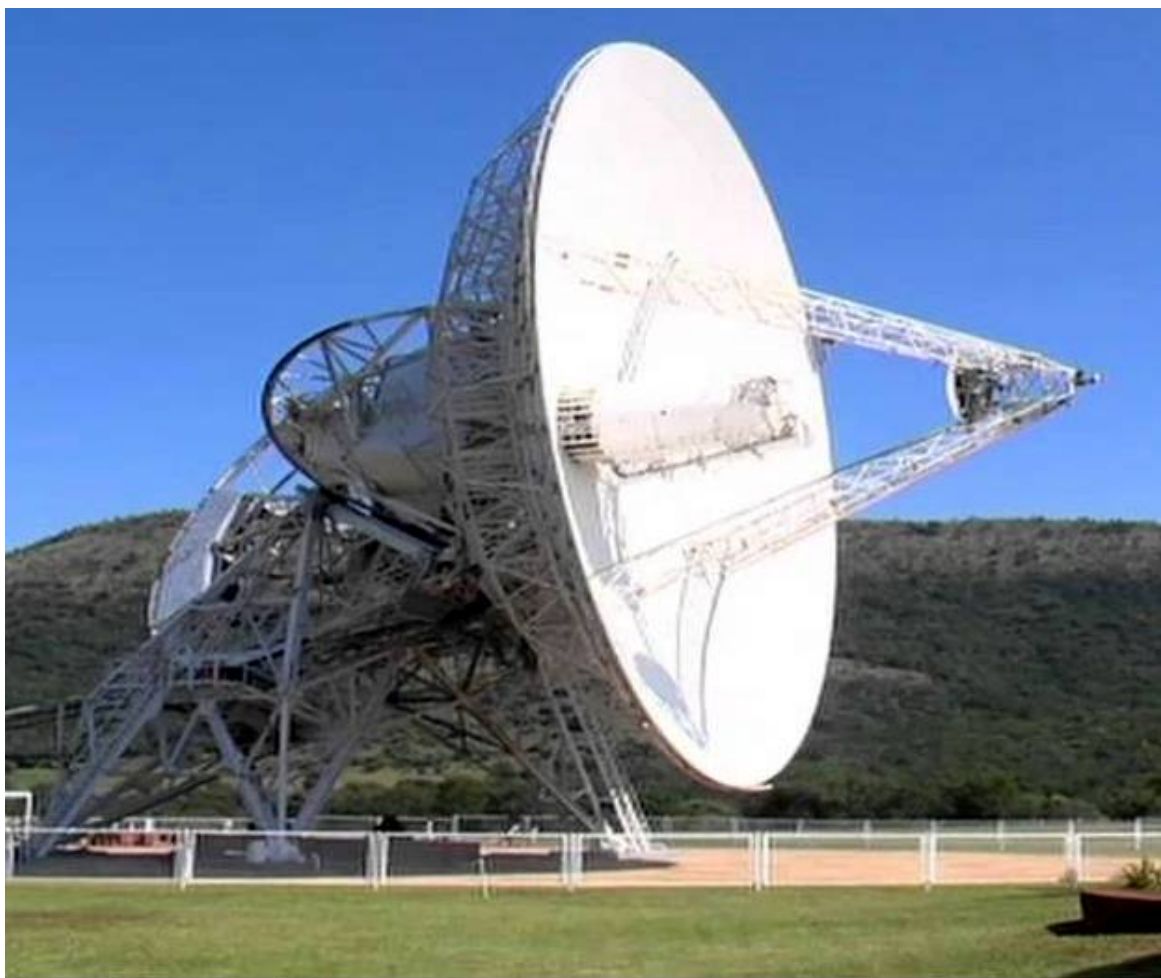


Figure 4: An image of the 26 m Hartebeesthoek radio telescope located in Krugersdorp, South Africa. (source: www.hartrao.ac.za)

Band	18 cm
Feed horn	1 × <i>circular</i>
Polarization	LCP and RCP
Amplifier	Cryogenic HEMT
Standard frequency	1666 MHz
Lower frequency	1608 MHz
Upper-frequency limit	1727 MHz
Receiver bandwidth	120 MHz
Beam-width: Full width at half max	0.494 degrees
Beam-width between first nulls	1.19 degrees
Minimum system temperature at Zenith	39 K
Point source sensitivity per polarization	5.1 Jy/K/Pol
System equivalent flux (SEFD)	430 Jy
Calibrator source	Hydra A

Table 2: Observing parameters for the Hartebeesthoek 26 m radio telescope (source: www.hartrao.ac.za)

The radio telescope design is Cassegrain with a focal ratio of 0.424, surface tolerance of 0.5 mm root mean square(RMS), wavelength limit of 1.3 cm, feed system type is Cassegrain, pointing resolution of 0.004 degrees and a slew rate on each axis of 0.5 degrees/s.

The observing parameters for the 1665 MHz OH transition frequency at HartRAO using the 26 m diameter telescope include a bandwidth of 1 MHz, velocity range of 45.0 km/s, correlator resolution of 0.044 km/s and root mean square (RMS) noise in 1 minute of 0.357 K or 1.84 Jy. Other observing parameters are summarized in table 1.

4.3 Observation Method.

The data used in this work was provided by HartRAO. The data used of NGC6334I range from 21 October 2011 to 14 December 2016. Observations were conducted every 5 to 10 days, depending on the availability of the telescope and the weather conditions. At times, observations were done on a daily basis while others were separated by weeks. Each observation on average comprised of two scans: ON the source and OFF the source. This technique is known as position switching. In position switching, the telescope is first pointed at the

target source (ON) before pointing at the cold sky (OFF). Each scan lasted for 150 s, therefore, a total of 300 s were spent per observation but only 150s on the source. So during each scan, the left and right circular polarization were recorded by the spectrometer back-end. To produce the final data for analysis, the data was processed and reduced in several steps.

4.4 Data Processing and Reduction.

First, the data was organized according to observational dates in their order before the processing and reduction started. It was reduced using an in-house program at HartRAO called *lines* which runs on Linux. Several steps were carried out which included, opening the terminal from which the data directory was accessed. Once in the directory containing the data, *lines* program was opened by typing the word 'lines'. To reduce one pair of data, a script called `reduce_1pr` was used. When the script `reduce_1pr` was run, it deleted all fits files in the data that were not part of a matched pair. The matched fits data files were then converted to comma separated values (csv) so that it can be read in the *lines* program. The script also removed any existing csv files before creating new ones. Once the csv files were created the script also created a list of all files to be read in *Lines* program. The csv files were read and plotted to an output screen showing the bandpass for both the LCP and RCP (see figure 4(a) to (d)). The first pair of bandpass was read and combined to create a spectra which was subsequently saved to the disc. The spectra created was saved in units Kelvin (K). If the data contained two or more pairs of data, appropriate script designed to reduce two pairs or more was used.

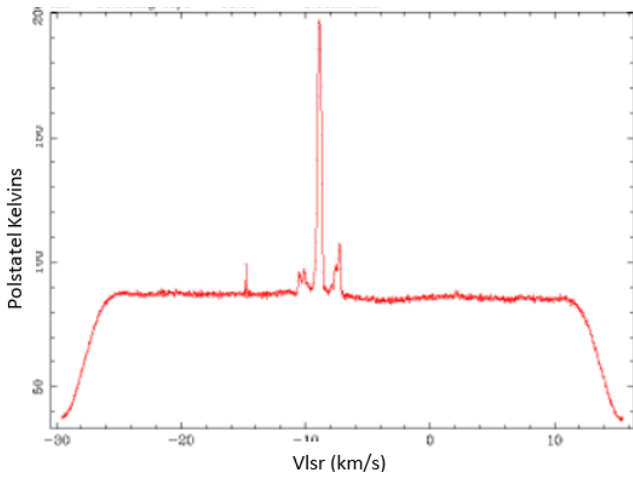
After data was reduced using the reduce scripts, the system temperature values were converted from Kelvin (K) to Jansky (J). This was done using *lines* and the script named `k2jy_oh1665` was used. The `k2jy_oh1665` script read the LCP spectra in Kelvin (K) and averaged it. The values of the system temperature were recorded to an excel spreadsheet according to the year, date and time of observation. The system temperature values were then converted to Jansky (Jy) using Hydra A as a calibrator source with a pointing source sensitivity (PSS) value of 5.2 Jy/K/Pol. This was also repeated for the RCP spectra, however a PSS value of 5.1 jy/K/Pol was used. The script was then used to flatten or correct the baselines. This was achieved by fitting a polynomial to the LCP spectra. The polynomial fitted was then subtracted to obtain a corrected spectra (see figure 4(e) and (f)). This process was done for both the LCP and RCP and the resulting spectra data was saved for further processing.

The steps outlined above were repeated for all the observational data and it was recorded on the excel spreadsheet according to year, date and time of observation and indicated if it contained radio frequency interference (RFI) or not. RFI was identified as a sharp and narrow spike on a plot of flux against velocity local standard of rest (V_{lsr}).

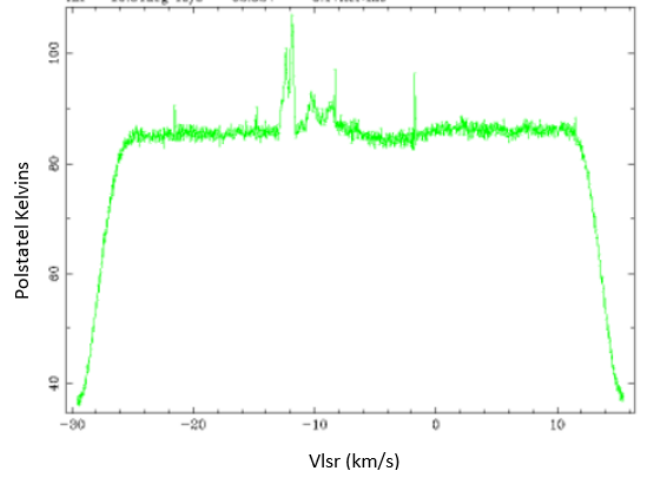
Once the baseline correction was done, the calculated flux for each dataset was entered into the excel spreadsheet for all observations separated into Left Circular polarization (LCP) and the right circular polarization (RCP) for velocity range of -29 kms^{-1} to 15 kms^{-1} and -33 kms^{-1} to 12 kms^{-1} . Since the data had two different velocity range, the one with a starting velocity of -33 km/s was adjusted and merged to match the one with an initial velocity of -29 km/s . Therefore, both LCP and RCP data were dealt with in the same manner.

Once the data reduction was completed, maser features were identified by means of fitting Gaussian to the spectra. This was achieved by the following steps:

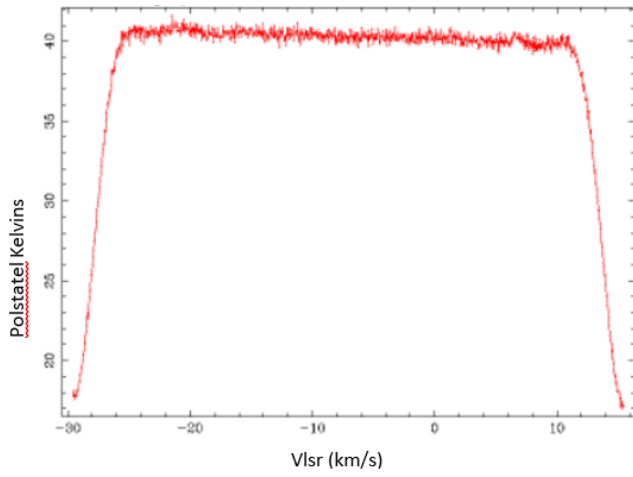
1. From the terminal, the directory containing the data was accessed from which *asc* files were listed using the command *ls .asc* <enter>.
2. *Lines* program was opened by typing *lines* then <enter>.
3. *asc* files in memory 1 were read using the command *ra .asc 1* and started a new average by typing Y to the pop-up question <Start new average?>
4. The results were then copied into memory 1 from 12 by using the command *cp 12 1*.
5. The second *asc* file was read and stored in memory 2 by typing *ra.asc 2* <enter>
6. Steps 3 and 4 were repeated but results were copied to memory 2.
7. Graphs of the data in memories 1 were plotted using the commands: *set plotdev /xw* <enter>. *pl 1* <enter> plots the first data in memory 1.
8. Polynomial of the appropriate order was applied to the bandpass in order to correct the baselines using the command *po [order] [Memory]*, where *po* is the polynomial, order of polynomial and the memory location respectively.
9. Velocity width was then set using the command *vw -18, 5, 1* <enter>
10. Identification of masers in memory 1 was achieved by fitting Gaussians to the spectra using the command: *gf 1* <enter>, this allows one to manually determine a maser



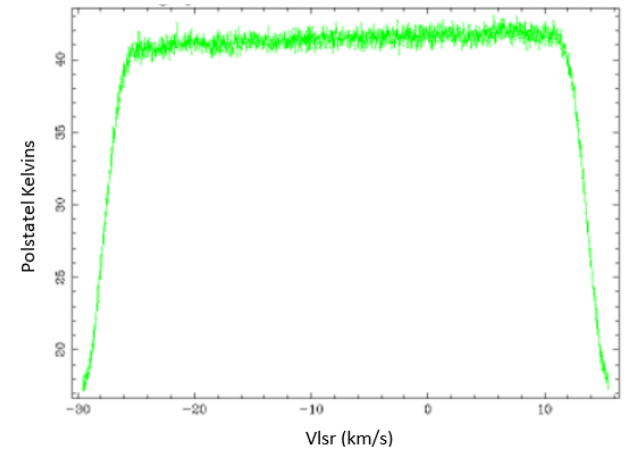
(a) LCP bandpass



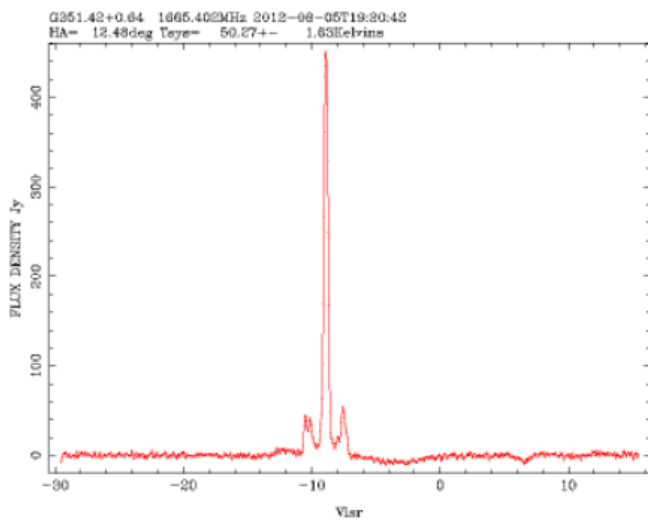
(b) RCP bandpass



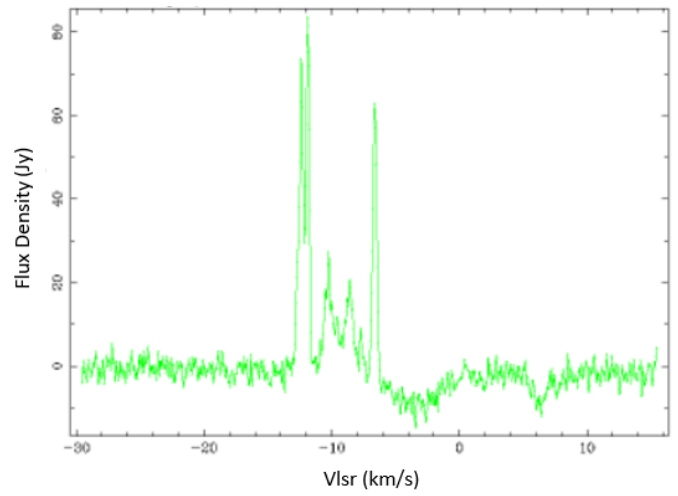
(c) LCP offsource



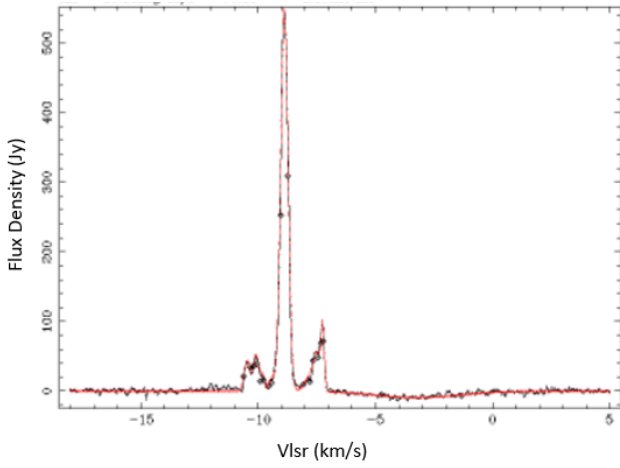
(d) RCP offsource



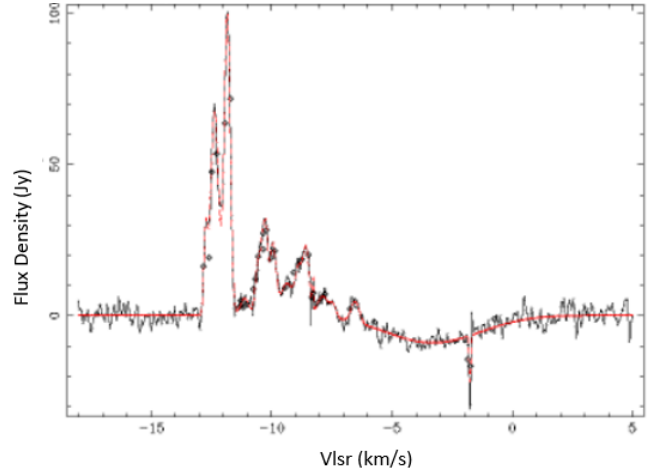
(e) LCP Maser profile



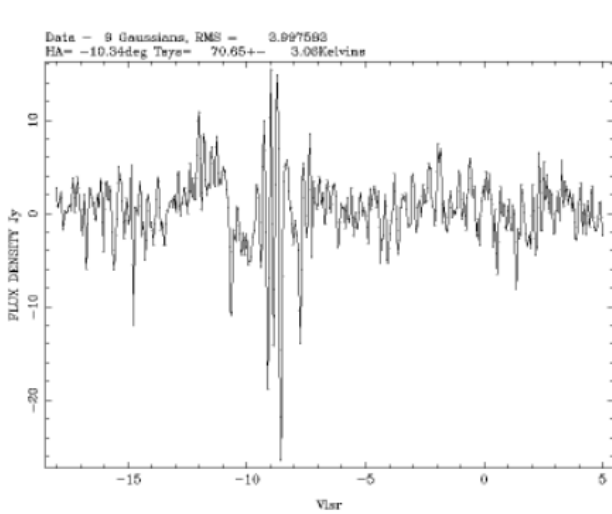
(f) RCP maser profile



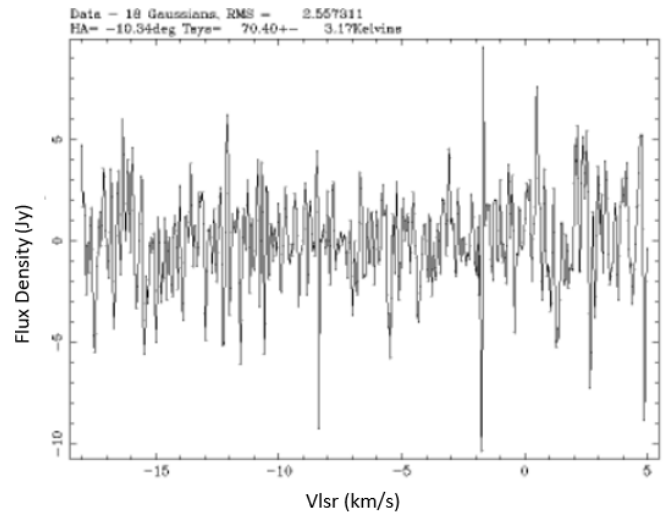
(g) Gaussian fit



(h) Gaussian fit



(i) rms noise



(j) rms noise

Figure 4: Stages in the spectral line data processing and reduction of 1665 MHz OH masers using the *lines* program for the left and right circular polarization (LCP and RCP).

Gaussian shape (see figure 4 (g)) and also remove RFI. The results were then copied and recorded on a notepad for both LCP and RCP.

11. Step 7, 8,9 and 10 were repeated for the data in memory 2.

The steps highlighted above were repeated for all the data from 2011 to 2016 and the results were recorded in an excel spreadsheet. Figure 4 sums up the stages involved in the data processing of spectral lines using the *lines* program.

4.5 Data Analysis

4.5.1 Pointing Check and Correction.

The pointing check of the telescope on the source was conducted in order to measure the accuracy of the pointing of the telescope. The observing technique used was position switching and it was assumed that the telescope beam was Gaussian. To check the pointing accuracy, The telescope was placed at half-power points, that is, the North, South, East, West and the center of the source NGC 6334I and the recorded bandpass is shown in figure 5. The North-South (N-S) spectra on figure 5 show that the half power of both the RCP and LCP were different as the telescope was pointed at the north and south of the source. As it can be seen from figure 5 that the half power for the LCP-North was less compared to that of the LCP-South, while on the other hand, the half-power of the RCP-North was more than that of the RCP-South. The same was observed for the East-West (E-W) pointing, only that the difference in the half-power are minimal compared to those of the N-S pointing (see figure 5). For the central pointing, it was observed that the half-powers were both the same as expected. The difference in the half-power between the LCP-North and LCP-South, RCP-North and RCP-South were attributed to the uncorrected baselines of the bandpass. In order to correct for the errors in pointing, the bandpass response and the residual baselines were corrected by applying a polynomial of order 3. Once the bandpass and residual baselines were corrected, the LCP and RCP pointing spectra were averaged according to their polarization using a python script. The averaged spectra for cardinal point and the center scans were plotted and are shown in figure 6.

Another python script (`reduce_1665_1on`) for conducting the pointing check was run using the *lines* program to determine the location of the masers whose velocity was varying periodically. This script was run for each of the velocities (-10.2 and -10.6 km s⁻¹) in the LCP that showed periodic variation in velocity to check for the location of the maser sources. The

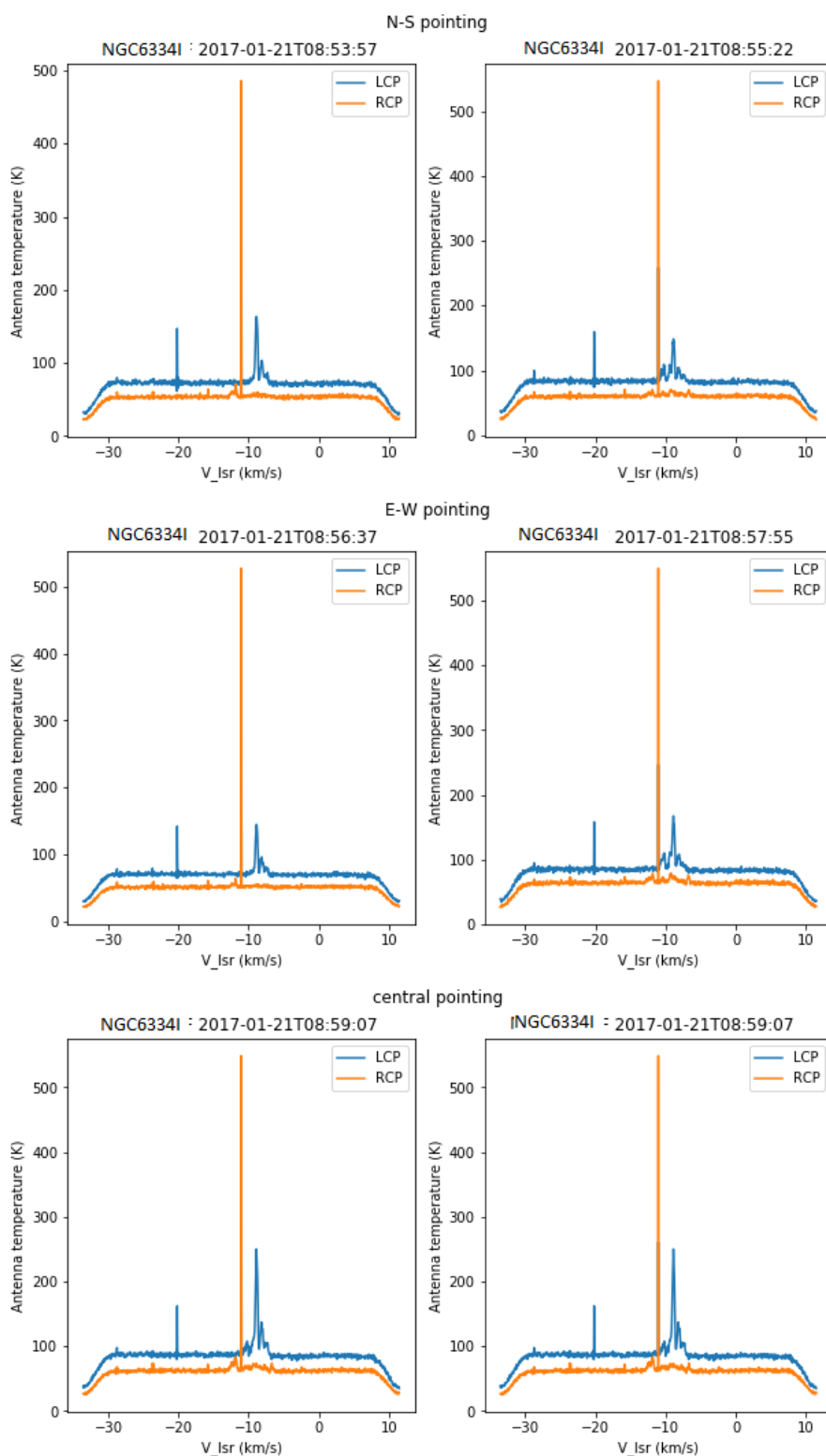
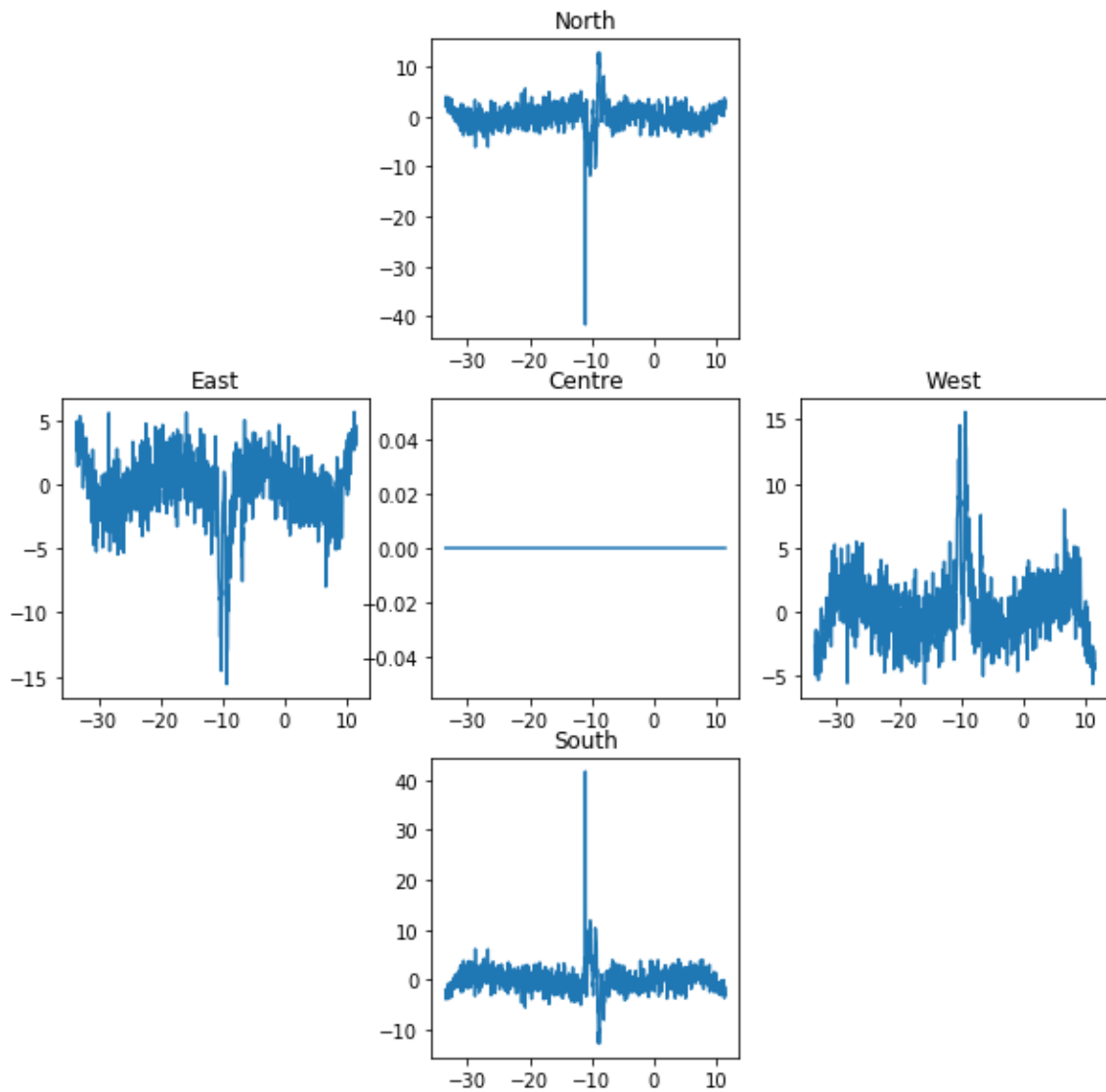


Figure 5: Images showing the telescope pointing scans for the source NGC 6334I for the cardinal points North-South, East-West and the center. Note that the bandpass and the baselines were not corrected yet for the above images



!ht

Figure 6: The pointing spectra for the North, South, East, West, and Central after bandpass response and residual baselines have been corrected and removed.

results were recorded in table 4 in the results section.

4.5.2 Determination of Period of Variability in Velocity.

A dynamic spectra of the 1665 MHz OH maser is shown in figure 7 for the October 2011 to December 2016 period. On the top panel we have the LCP dynamic spectra while on the lower panel we have the RCP dynamic spectra. The vertical black line marks the date when a flare was first observed in Methanol masers as reported by MacLeod *et al.*, 2018 while the dotted line approximate the date the 1665 MHz OH maser started flaring.

Modified Julian dates were calculated using the following equation:

$$MJD = Date + Time + 3415018.5 - 2450000.5 = JD - 2450000.5 \quad (9)$$

where JD is the Julian Date.

To visualize how the flux and the V_{lsr} were varying with time (Days), a dynamic spectra was plotted for the LCP and RCP using python and are shown on figure 7.

It can be seen in the top panel of figure 7 that between a velocity of -11 km s^{-1} and -10 km s^{-1} there are two maser features showing possible periodic variation in their velocity in LCP. In addition, in the RCP spectrum between -7 km s^{-1} and -6 km s^{-1} there is another feature showing the same behavior. The variations are hereafter referred to as wiggly. However, it can be noticed that the wiggly line in the RCP fades away. The nature and cause of the wiggly are discussed in the results section

To analyse and understand why these maser features vary in velocity and what the period of variation is, gaussian fitting was applied to each maser feature of every observation from 2011 to 2016. In particular these velocity varying features at -10.6 and -10.2 km s^{-1} in LCP and the -6.7 km s^{-1} velocity feature in RCP. Figure 8 shows the gaussian fitted velocity of the three maser features at their peak flux density.

For the plots showing periodicity, a sine function was fitted to the data (see figure 9) in order to determine the period of variation. A computer program Period04 was used to do the fitting and for more information about this program see Appendix A2. The following stages were followed while using Period04. First, the velocity and the time string (MJD) were copied and saved as text files. The data was loaded into Period04 using *Import string* tab. To obtain the first frequency and amplitude, a Fourier transform of the data was done and the calculations were based on the loaded original data. The frequency obtained was used to do the fitting.

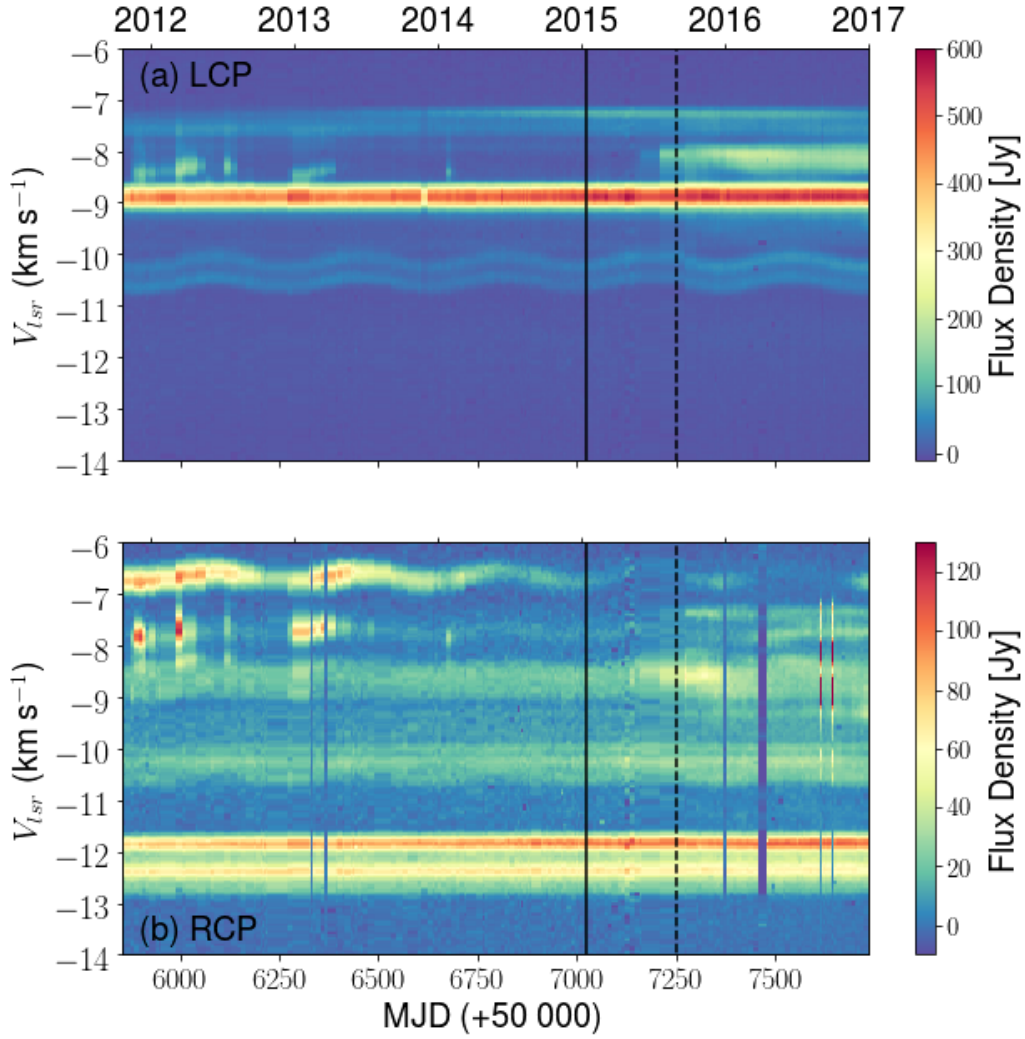


Figure 7: Dynamic spectra of the 1665 MHz OH maser showing the variation of velocity with time on the scale of days as obtained from each day of observation

The equation used for the fit was a sine function

$$y = z + \sum A_i \sin(2\pi(\Omega_i t + \Phi_i)) \quad (10)$$

where A is the amplitude, Ω is the frequency, t is the time and Φ is the phase

The calculated frequency was then selected and used in the phase calculation and parameter improvement, giving the best frequency, amplitude and phase. The second stage involved calculating the frequency of the residuals which was also used in the fits to improve the values of the frequency, amplitude, and Phase. Once these parameters were determined, the period (T) was calculated using the equation:

$$T = 1/\Omega \quad (11)$$

where Ω is the frequency. This method was used to determine the period of the wiggly lines. The results were recorded in table 2 in the results section.

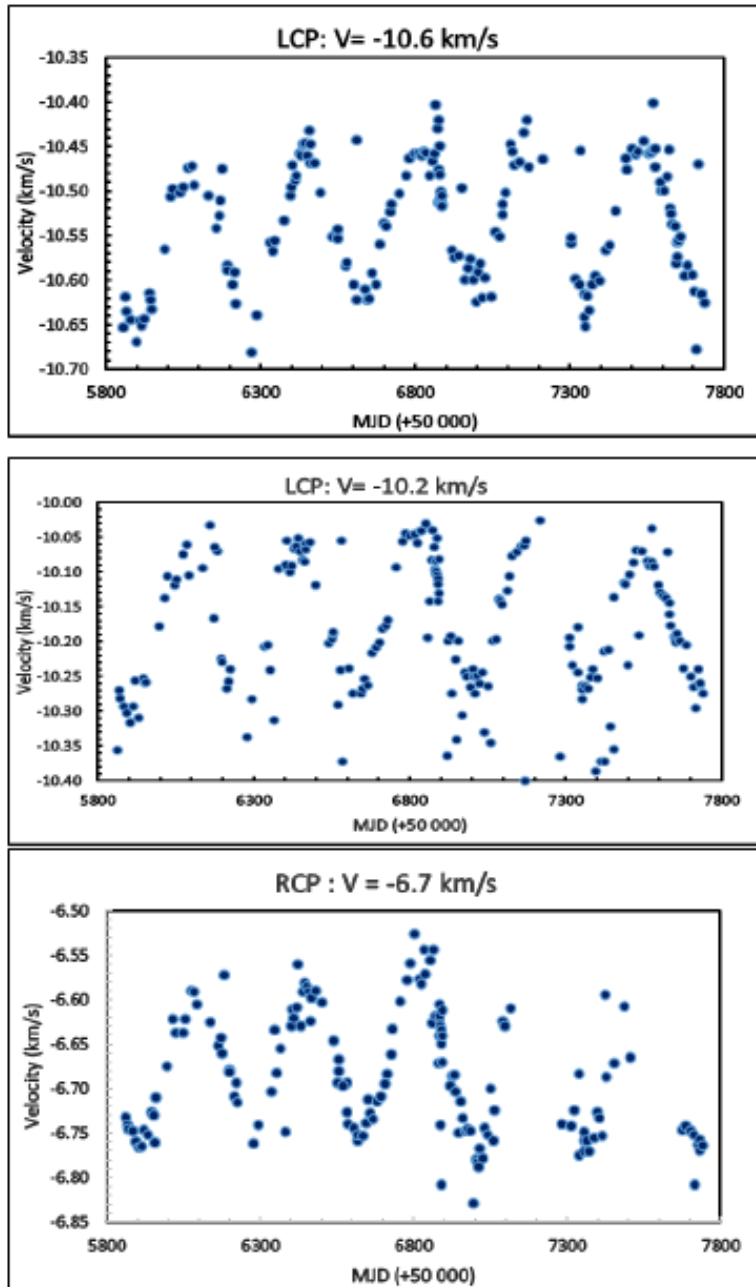


Figure 8: Time series plots showing variation in velocity of the 1665 OH maser associated with NGC 6334I for both the LCP and RCP. In the RCP the OH maser varies periodically at about a velocity of -6.7 km s^{-1} while in the LCP the variation occurs at -10.2 km s^{-1} and -10.6 km s^{-1} .

4.5.3 Approximation of Angular Separation of Maser Sources Causing Periodic Variation

To approximate how far the maser source was from the target source, V_{lsr} values were calculated using an online calculator called Velocity/VLSR/Observation Frequency Calculators. In this calculation, the telescope coordinates used were: Latitude $25^{\circ} 53' 14''.4$, Longitude $27^{\circ} 41' 05''.2$. While those used for the target source (NGC 6334I) were; Declination $-35^{\circ} 47' 1'$ and Right Ascension $17^h 20^m 53^s.4$. The rest frequency chosen was 1665 MHz for the OH maser. The values of the declination were increased by an interval of $5'$ and the value of the V_{lsr} were calculated for each day of observation.

The V_{lsr} values obtained were then recorded in excel spreadsheets for angular separation from $5'$ to $55'$. The V_{lsr} values were then plotted against the MJD and fitted with equation 10 in order to determine its frequency, amplitude and period of variation using Period04. The results obtained were recorded in table 3.

4.5.4 Removal of Infringing Masers From The Dynamic Spectra

Three lines of 1665 MHz OH masers were identified to undergo periodic variation of which two were in the LCP and one in the RCP (see figure 11 a). These lines were observed at velocities -10.6 km s^{-1} and -10.2 km s^{-1} in the LCP and -6.7 km s^{-1} in the RCP. Maser features at these velocities were identified to originate from NGC 6334-V which is far away from our target source (NGC 6334I). As a result, they were removed from the dynamic spectra shown on figure 11 for the LCP so that further analysis could be done more effectively.

In order to remove the infringing masers (see figure 11 a), a python script was created which enabled us to load maser spectral data from observations and fit two Gaussian to maser features positioned at -10.6 km s^{-1} and -10.2 km s^{-1} velocities in the LCP. While doing the fitting, the values of the amplitude (maser height), the mean (the center velocity) and the width (standard deviation) were adjusted until a good fit was obtained. The spectral data generated by fitting Gaussians was recorded to a file. This procedure was repeated for each epoch of observation. The spectral data obtained from fitting Gaussians for all epochs was then subtracted from the original observational data. The subtraction removed most of the infringing masers originating from a nearby source NGC 6334-V. The results of this process are in the results and discussion section.

4.5.5 Identification of Zeeman Pairs and Magnetic Field Calculation

The data used in this research was obtained from a single dish observations. This means that identification of Zeeman pairs using the Stokes V spectrum as it is generally the case, could not be used. Instead we looked for maser spectra for the RCP and LCP that were similar and appeared to have been varying in a similar way in velocity or in flux density. Using this approach, a Zeeman pair was identified at -10.12 km s^{-1} and -11.83 km s^{-1} (see figure 12) in the LCP and RCP respectively. These pairs had a similar maser spectra despite the difference in their flux density. To obtain the values of Δv_z (see equation 4 and 8), velocity value for the maser spectra were subtracted by using the relationship $V_{RCP} - V_{LCP}$. The magnetic field was then calculated using equation 12.

$$\mathbf{B}(mG) = \Delta v_z / b \quad (12)$$

where Δv_z is the difference in the velocity between the RCP and LCP along the line of sight, while $b = 0.59 \text{ km s}^{-1} \text{ mG}^{-1}$ is a constant for 1665 MHz OH masers (Fish *et al.*, 2003). The results obtained from the calculation are found in the results section.

5 CHAPTER FIVE: RESULTS AND DISCUSSION

5.1 Introduction

The findings of the study in-line with the objectives, Methodology and data analysis are presented in this chapter. Each of the results are first presented and then discussed in that order.

5.2 Variability in V_{lsr} .

The plots of velocity versus Modified Julian Dates (MJD) showed no variation in velocity for both the LCP and RCP except for maser features positioned at -10.6 km s^{-1} and -10.2 km s^{-1} (in the LCP) and -6.7 km s^{-1} (in the RCP) as can be seen in figure 7. The affected velocity channels were fitted with a sine function and the values of period and amplitude were determined.

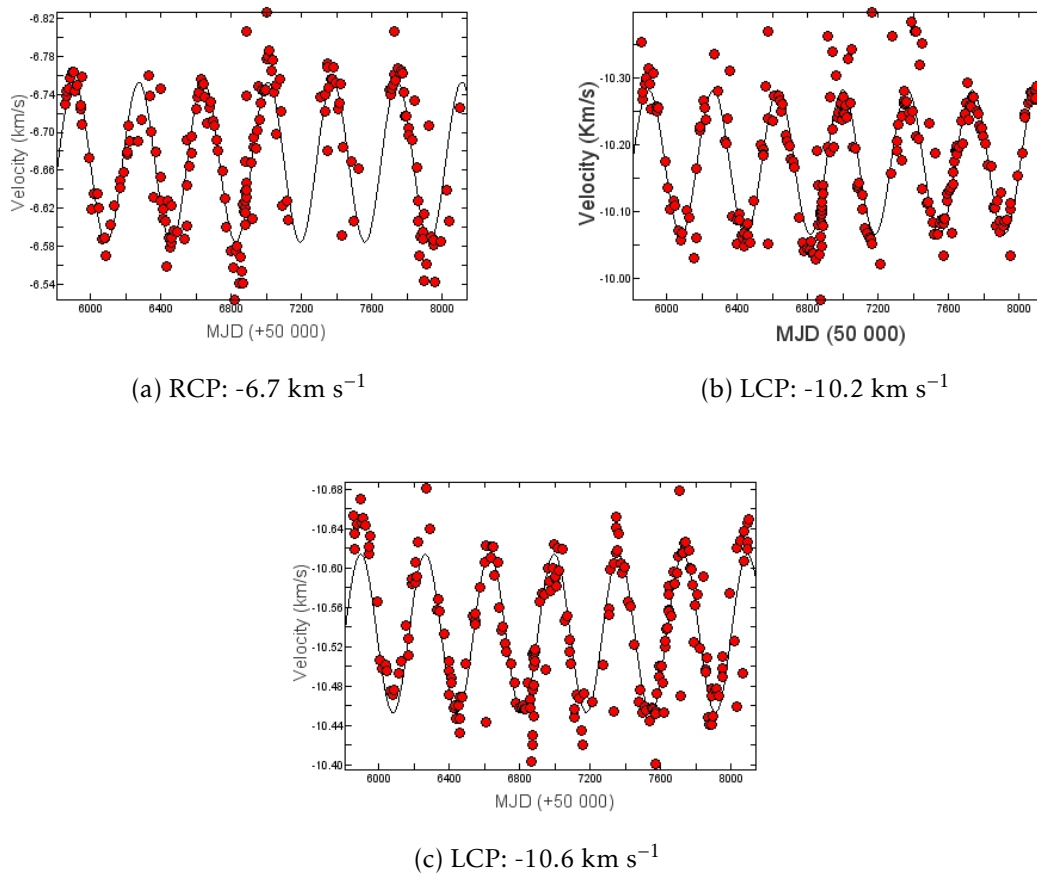


Figure 9: Plots (a), (b), and (c) are variations in the velocity of 1665 MHz OH maser observed towards NGC6334I

The period of variation and amplitude of the 1665 MHz OH masers associated with NGC 6334I are present in table 2. It can be observed that the period of variability are within the error to that which the earth takes to orbit the sun which is 365 days. This may suggest that the variation was caused by maser sources that are within the telescope view angle but far enough from the target source (NGC 6334I). As a result, the V_{lsr} corrections made during observations to fix the position of the telescope with respect to the sun and the source for each day of observations were not effective for those sources further away from the NGC6334I and hence the noticed periodic shifting.

The variance observed in velocity for the LCP corresponding to -10.6 and -10.2 km s⁻¹

Table 3: Results of period and amplitude calculations using period04 for the 1665 MHz OH maser associated with NGC 6334I obtained from observational data.

Polarization	Velocity(km/s)	Amplitude	Frequency (f)	Period (T)[in days]	ΔT
LCP	-10.6	0.0794965469	0.00273217921	366.01	± 3.33
LCP	-10.2	0.103577915	0.00273302937	365.89	± 1.28
RCP	-6.7	0.0853705707	0.00272711396	366.69	± 1.38

about their central position was 0.079 km s⁻¹ and 0.103 km s⁻¹ respectively. However, the rest of the maser features appear to be non-variable as it relates to velocity. Now for the RCP data, the velocity varied about its central position (-6.7 km s⁻¹) by 0.085 km s⁻¹. The measure of the variance in velocity gave us an idea of how far the maser feature showing variation is from the target source (NGC 6334I).

The major cause of variation in velocity is the doppler shifting usually caused by misalignment of the maser column along the line of sight (Caswell., 1997). Most of these variations are dealt with using the software during data processing. As a result, they do not cause periodic variation such as that observed in our case. The expected variability of the masers in velocity from the beam center is usually less than 2 % , that is beyond 30 arc-minutes away from the target source. However, in our case, a variation of about 8–10 % was observed in the velocity and this was significant and would need to be resolved by either removing them after observation or employing V_{lsr} corrections for their source.

5.2.1 Approximation of Angular Distances Using Calculated V_{lsr}

The likely cause of periodic variability in velocity observed towards NGC 6334I maser features was that the Velocity local standard of rest (V_{lsr}) were not corrected according to their

galactic position, it is possible to approximate the angular distance or separation between our target source (NGC 6334I) to the unknown sources. This was made possible by calculating V_{lsr} for 1665 MHz OH molecular transition associated with NGC 6334I for each day of observation, making light curves fitted with the same sine function (equation 10) used to determine the period of variability and by comparing their amplitudes. The results were recorded in table 3

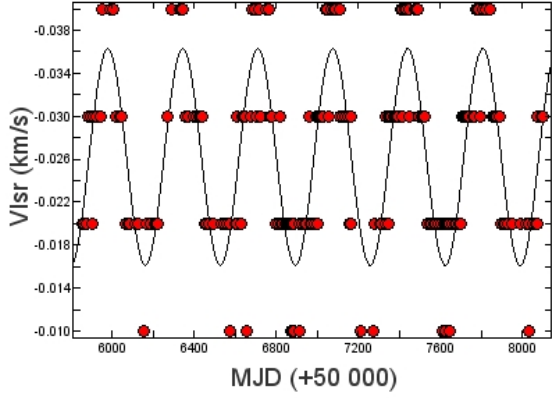
Comparing the values of amplitude between those in table 2 and 3, it was clear that our maser sources causing the periodic variation in V_{lsr} were found at some distance 40' in the case of $V_{lsr} = -10.6\text{km s}^{-1}$, 50' for -10.2 km s^{-1} and 42.5' for -6.7 km s^{-1} . From these values it can be noted that the masing species are quite some distance away from NGC 6334I and as such could have caused the periodic variation.

Table 4: V_{lsr} correction values using period04 for the 1665 MHz OH maser associated with NGC 6334I

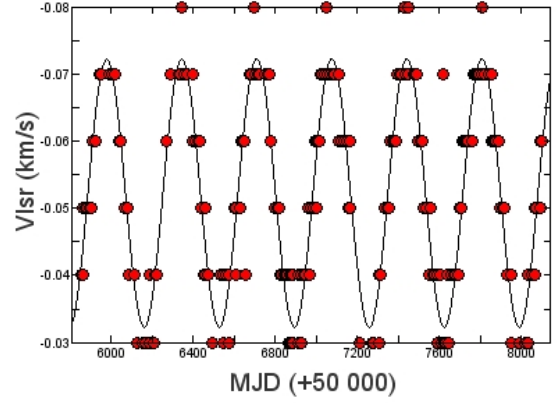
Angular separation(arcmin)	Amplitude	Frequency (f)	Period (T)[in days]
5	0.009988985	0.00273735701	365.32± 1.24
10	0.0200158798	0.00273401626	365.76± 0.85
15	0.030503197	0.00273795586	365.24± 0.41
20	0.0400419309	0.00273414333	365.75± 0.42
25	0.0521255162	0.00273780057	365.26± 0.31
30	0.0599922214	0.00273791369	365.24± 0.29
35	0.0701646436	0.00273910237	365.06± 0.29
40	0.0806121847	0.00273756673	365.29 ± 0.22
45	0.091234401	0.002736999090	365.36 ± 0.20
50	0.1011307296	0.00273938615	365.05 ± 0.15
55	0.112212114	0.00273520376	365.60 ± 0.12

5.2.2 Pointing Check results

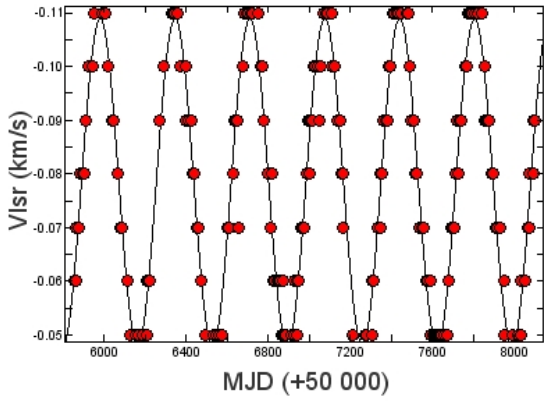
The pointing check was performed on the 21 September 2017 in order to find out if the periodic shifting in velocity was due to pointing errors. Using the *lines* software along with



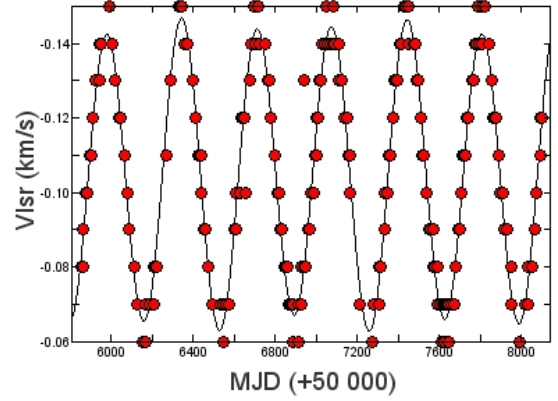
(a) Distance: 5'



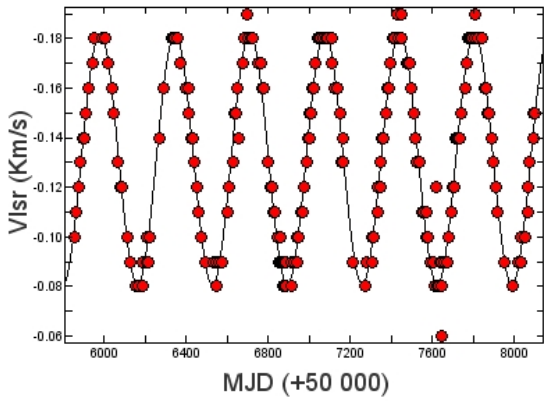
(b) Distance: 10'



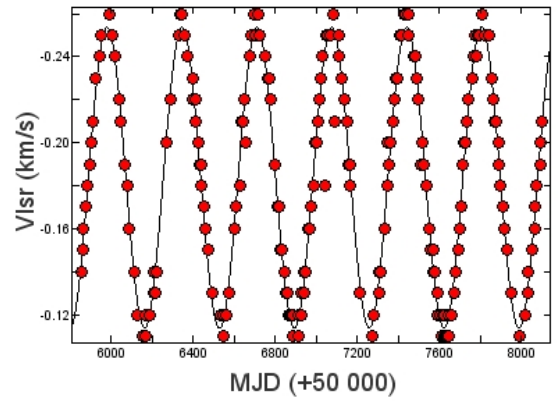
(c) Distance: 15'



(d) Distance: 20'

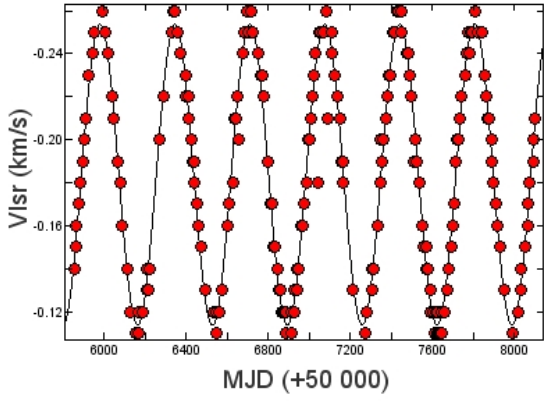


(e) Distance: 25'

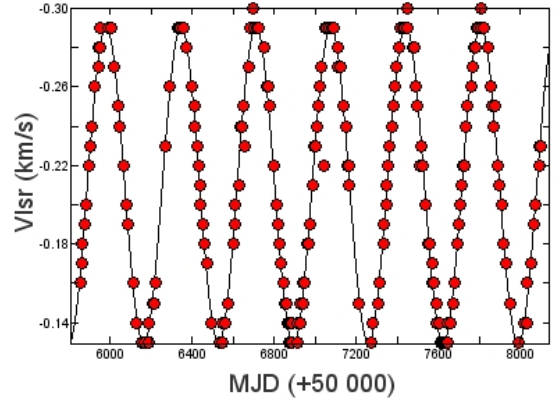


(f) Distance: 30'

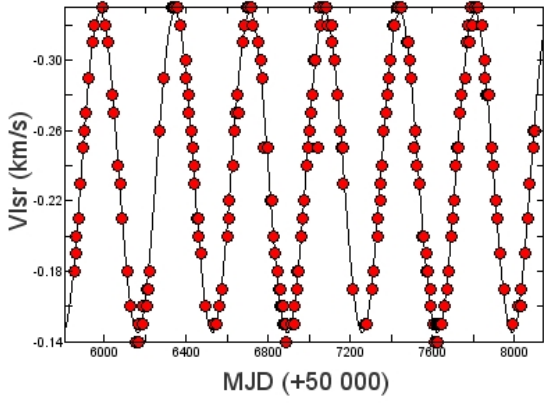
a python script, a pointing check was done for velocities -10.2 km s^{-1} and -10.6 km s^{-1} . The results of the pointing check were recorded in table 4. From the information in table 4, it can be noted that there was a significant separation in the position of the field center (NGC 6334I) from the position at which masers with velocity -10.25 km s^{-1} and -10.60 km s^{-1} were found.



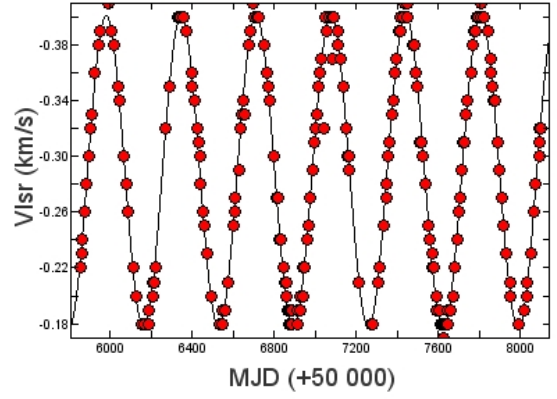
(g) Distance: 50'



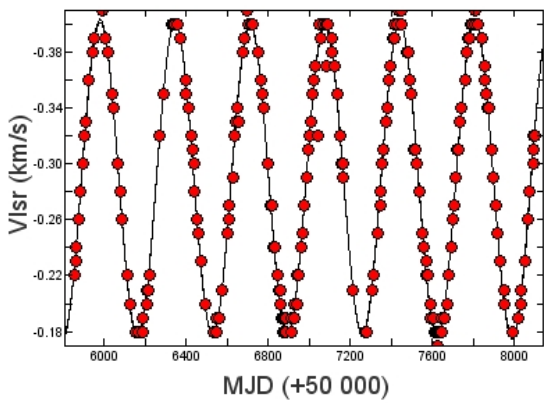
(h) Distance: 40'



(i) Distance: 45'



(j) Distance: 50'



(k) Distance: 55'

Figure 9: Light curves of V_{lsr} for the 1665 MHz OH maser calculated at varying distances from NGC6334I for each day of observation and fitted with a sine function.

Table 5: Pointing parameters and the associated errors conducted on 21 September 2017 for specific 1665 MHz OH maser velocities that showed periodic variation in the LCP

Field Center (NGC6334I)	Velocity (km s ⁻¹)	Varying Maser Position	Difference (deg)
RA (1950):259.3833	-10.25	17 ⁰ 16 ^m 51 ^s .9	
DEC(1950):-35.7339		-35 ⁰ 53' 26''.4	
RA (1950)		259.216 (deg)	Δ RA: -0.166(deg)
DEC(1950)		-35.891	Δ DEC: -0.183 (deg)
Longitude (l): G351.417		G351.211	
Latitude(b): 0.646		0.667	
RA (1950)	-10.60	17 ⁰ 16 ^m 43 ^s .0	
DEC(1950):		-35 ⁰ 55' 2''.5	
RA (1950)		259.179 (deg)	ΔRA: -0.166 (deg)
DEC (1950)		-35. 917 (deg)	Δ DEC: -0.183 (deg)
Longitude (l)		G351.171	
Latitude(b)		0.676	

Using the information of the RA and DEC for the masers showing periodic variation in the LCP, we were able to identify the maser sources which caused periodic variation in our observations.

In figure 10, we have an image of the complex molecular cloud of NGC 6334 as seen at 1.6 GHz continuum emission using the Australia Telescope Compact Array (ATCA). There are 9 active star-forming regions including our target source (NGC 6334I). From figure 10 we approximately identified the maser source that caused periodic variation at -10.25 km s⁻¹ and -10.60 km s⁻¹ in the LCP to be NGC 6334-V. This region is located at RA (1950): 17^h 16^m 39^s.50 and DEC (1950): -35⁰ 53' 05''.9 (Brooks & Whiteoak, 2000) while the source that produced the masers with velocity -10.25 km s⁻¹ and -10.60 km s⁻¹ was located at RA(1950): 17^h 16^m 51^s.9, DEC(1950): -35⁰ 53' 26''.4, and RA(1950): 17^h 16^m 43^s.0, DEC(1950): -35⁰ 55' 2''.5 respectively.

By comparing the locations obtained from the pointing check conducted on 21 September 2017 of the maser source causing periodic variation and those on figure 10, we were able to identify the source NGC 6334-V as the maser source which produced the infringing masers that caused periodic variation at -10.2 and -10.6 km s⁻¹. NGC 6334-V is found South of NGC 6334I (see figure 10) and is far enough that the V_{lsr} that were used during observation

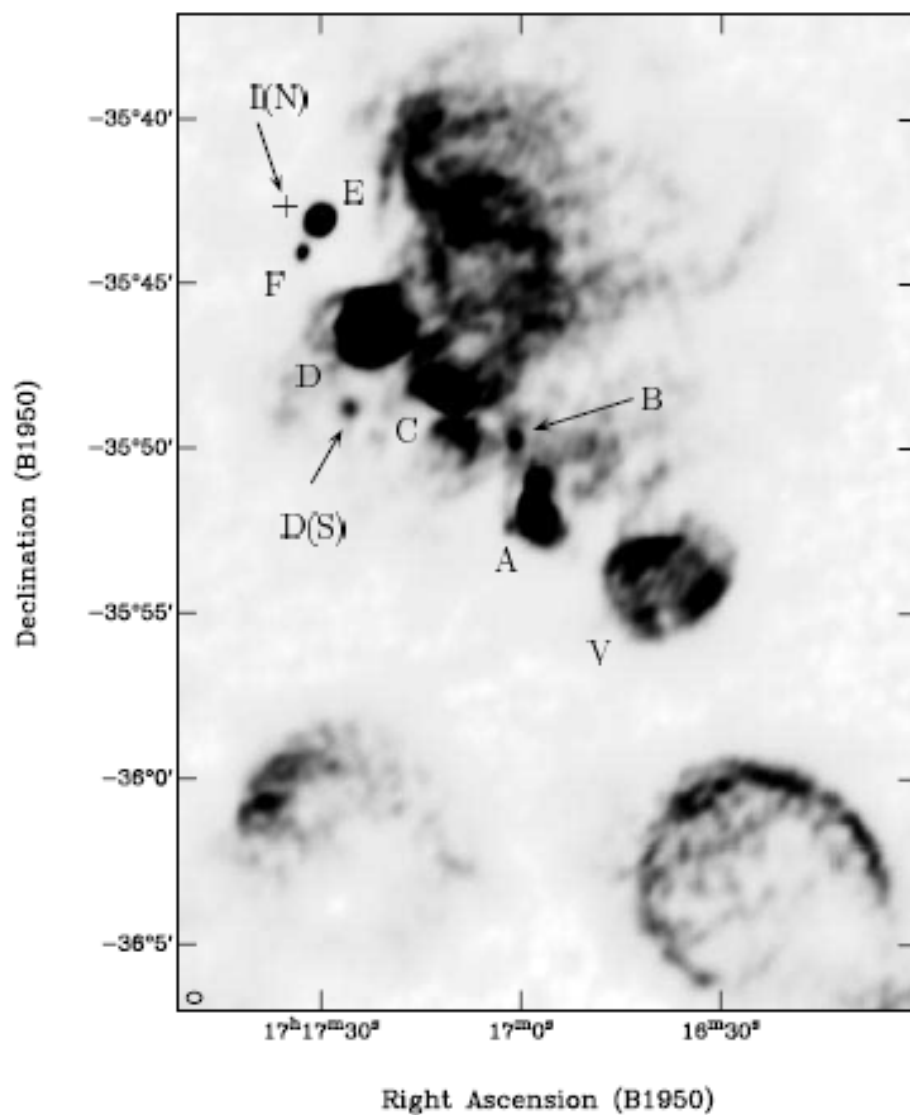


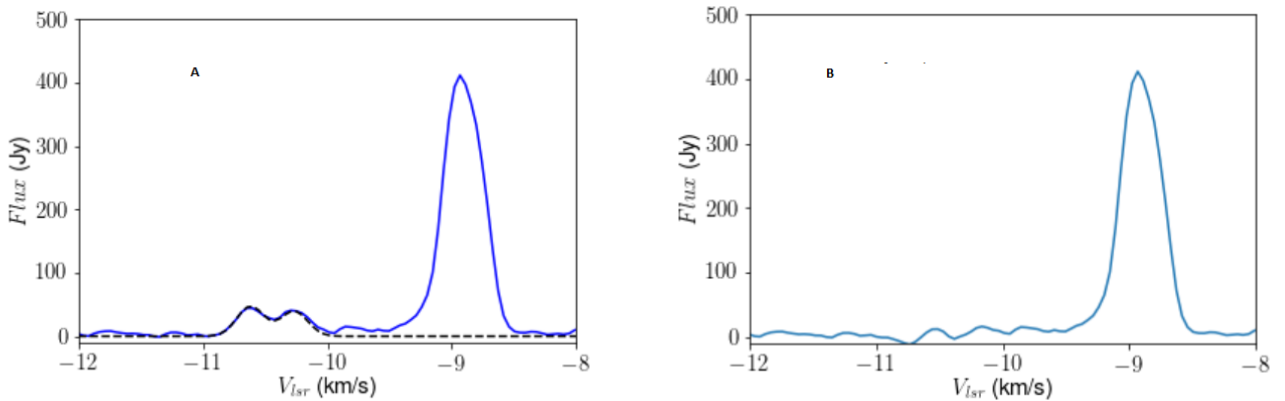
Figure 10: Image showing continuum emission of multiple star-forming regions in NGC6334

source: Whiteoak & Brooks, 2000

did not take effect for masers originating from this source. Since there was no sufficient RCP data on the pointing check, it was not possible to identify the maser source that caused periodic variation of 365 days at -6.7 km s^{-1} .

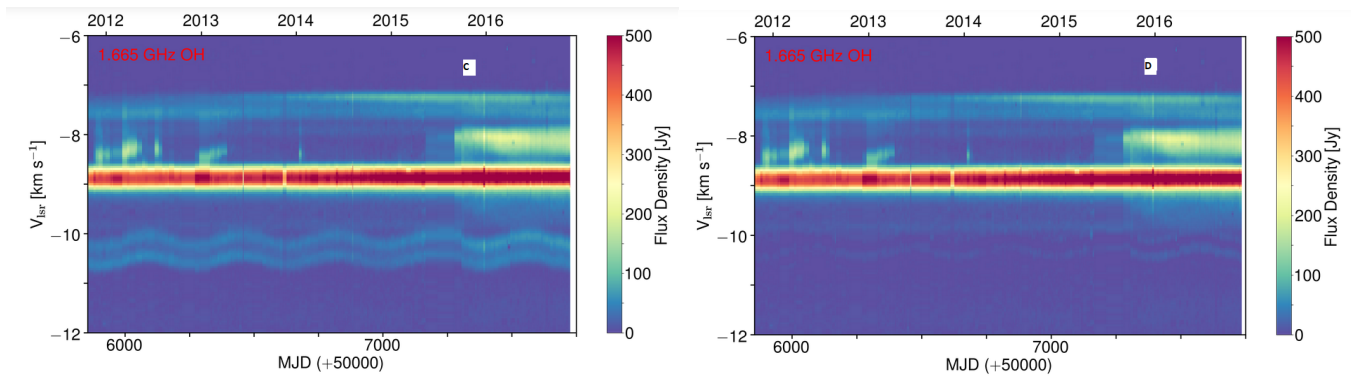
5.2.3 Removal of Infringing Masers Results

Infringing masers from nearby sources during single dish observations can be successfully removed from the data. In our case, a nearby source NGC 6334-V caused some maser features at peak velocities -10.6 and -10.2 km s^{-1} to undergo periodic variation in velocity features. Most of the periodically varying features were successfully removed using pyphon scripts and the images of results are shown in figure 11. In figure 11 (a) on the left-upper panel is a partial spectra showing maser features fitted with Gaussians at the above mentioned peak velocities and in figure 11 (b) on the right-upper panel is the resulting spectra after the fitted maser features were subtracted. Figure 11 (c), on the left-lower panel is



(a) Gaussian fitted spectra

(b) Fitted spectra removed



(c) Dynamic spectra before removal of periodic features

(d) Dynamic Spectra after removal of periodic features

Figure 11: Images showing the process of removing infringing masers in NGC 6334I.

a dynamic spectra showing the periodically varying features in velocity before it was removed and figure 11(c) on the right-lower panel is a dynamic spectra after the infringing masers, the ones showing periodic variation were removed through subtraction. However, it can be seen from figure 11 (d) that not all the periodically varying maser features were removed. This simply suggest that there are still masers originating from the nearby source NGC 6334-V present in the data and they are mainly positioned near -10.0 km s^{-1} peak velocity. These maser features are quiet faint and could be removed further by repeating the procedure on section 4.5.4 to the subtracted spectra (see figure 11(b)) for all epochs of observation.

5.3 Flaring of 1665 MHz OH Maser in NGC 6334I

Apart from variations observed in the velocity of the 1665 MHz OH maser features associated with NGC 6334I, the source also had significant flaring events which were first observed in the 6.7 GHz methanol transition (MacLeod., *et al.*, 2018) and later in OH and water masers. In this case, flaring refers to an increase in the flux density of the maser spectra.

Figure 11 (a) show images of velocity channels, Modified Julian Dates and flux density plotted in a dynamic spectra. As we can see from the color bar scale on the right in figure 11 (a), the regions in blue have the lowest flux and the redder it is, the higher the flux density. We can, therefore, notice a high value of flux just around the velocity channel of -9 km s^{-1} . This flux density eventually changes or increases its intensity (it flares) starting from around 2015. A similar change is also noticed in the RCP plots, however, the flaring is less compared to that in the LCP.

The solid vertical line in figure 11 (a) approximates the date on which the flaring began to be observed in the methanol maser at 6.7 GHz as reported by MacLeod *et al.*, (2018). To have a closer look at how the flux of various velocity channels changed with time, some time series were plotted using python and the images are shown in figure 12 . Figure 12 (a) are plots of the 1665 MHz OH maser profile for the LCP for the dates 10 January 2015, 15 September 2015 and 25 August 2016 which clearly show that the masers increased in intensity by about a 50 Jy thats between 2015 January and August 2016. Figure 12 (b) is a plot of Gaussian fitted OH maser profiles at the indicated velocity channels. Masers positioned at velocities -8.19 and -7.92 km/s show a significant increase in flux especially after 57023.5 MJD. The solid vertical line (57023.5 MJD) corresponds to the date just prior to the start of the observed flaring. The dotted vertical line at 57239.5 MJD marks the approximated start

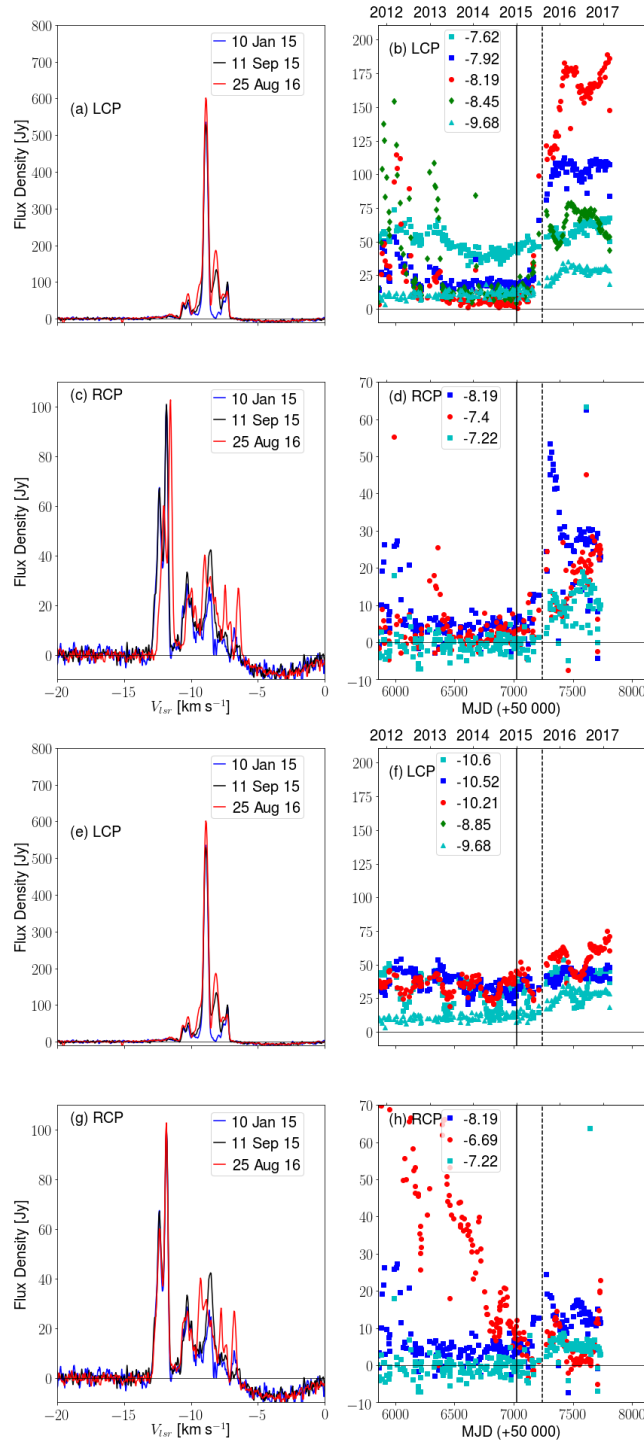


Figure 12: image of time series showing the variation of flux with time in the LCP and RCP at various velocity channels

date of the 1665 MHz OH maser flaring which correspond to 216 days after the 6.7 GHz methanol maser flare.

Coming to figure 12 (c), it can be noticed that not all the velocity channels were affected by the flaring on the above mentioned dates except for those near -7.4 km s^{-1} and -8.19 km s^{-1} . These are clearly shown in figure 12 (d) where we notice a substantial increase in flux density

at the velocity channels -7.4 km s^{-1} and -8.19 km s^{-1} . It can be noticed from figure 12 (d) that the flaring began almost the same time for both the RCP and the LCP. Similar flaring was observed and reported by MacLeod *et al.*, (2018) in methanol masers that it began on January 10, 2015.

Masers that showed periodic variation in velocity were also investigated to find out if they also flared. It was found that the 1665 MHz OH maser with a velocity of -10.21 km s^{-1} in the LCP increased gently in flux and also varied periodically in the flux (see figure 12 (f)). On the other hand, the maser found at -10.52 km s^{-1} decreased in flux density from 50 Jy to about 40 Jy. In the RCP, we found out that the maser with a velocity of -6.69 km s^{-1} decreased rapidly in its flux density from 70 Jy to almost zero by January 10, 2015 (see figure 12 (h)). The two masers found at -10.52 and -6.69 km s^{-1} in the LCP and RCP would be Zeeman pairs because they both exhibit similar periodic variation in velocity with the same error margin in period. As a result, it can be used as an additional criteria for estimating the magnetic field strength in star forming regions. This Zeeman pair gives a magnetic field strength of $6.14 \pm 0.3 \text{ mG}$. The orientation of this magnetic field is away from our line of sight which can be attributed to the fact that the measured magnetic field was for nearby region NGC 6334-V

The cause of the unprecedented flaring observed towards NGC 6334I are not obvious. Hunter *et al.*, (2017), suggested that the outburst of flux density could have resulted from an increase in the dust temperature which in turn caused an increase in the radiative pumping of various maser emissions in NGC 6334I. Even though there is a relationship between the increase in dust temperature and maser emission, it does not explain the cause of the increase in the dust temperature as well as the the observed flaring of 1665 MHz OH maser.

On the other hand, Hunter *et al.*, (2017) proposes the occurrence of an accretion event similar to an FU Ori outburst which typically takes place in low mass proto-stars in which the luminosity of accretion drastically increases followed by long term decays (Hartmann & Kenyon, (1996)). The first observed outburst in high mass proto-stars was recently reported by Caratti O Garatti *et al.*, (2017) which coincides with an extended methanol maser flare (Moscadelli *et al.*, 2017). For such an accretion event to heat up the dust in NGC 6334I-MM1 (see figure 1) by the observed amount it would take about 200 days (Hunter *et at.*, 2017) of which the calculations were based on equations of Johnstone *et al.*, (2013).

A near encounter of one protostar with another or a merger would also trigger an accretion event that would cause the flaring (Hunter *et al.*, 2017). Bally & Zinnecker (2005), suggested that stellar mergers in our galaxy would occur at the same rate as the that at which

massive stars are born which would result in high luminosity infrared flares which may then pump OH and methanol masers and the shocks associated with them would pump the water masers.

It is expected that different maser species and velocity components would turn on at different times during the period of the heating. This is because different maser species and transitions are found in different local geometries and opacity surrounding the dense medium. As a result, we notice that the 1665 MHz OH maser transition flares after about 220 days after the methanol maser (MacLeod *et al.*, 2018). Recent VLA observations reported by Hunter *et al.*, (2017) confirmed methanol masers transitioning at 6.7 GHz and excited OH masers transitioning at 6.0 GHz are spatially associated with NGC 6334I-MM1 and CM2 which are both consistent with variations associated with features of the 1665 MHz OH maser spectra just observed.

To support the FU Ori-like origin hypothesis for the flaring observed in the 1665 MHz OH maser, we compare it to the outburst in the 1720 MHz OH maser associated with the 5.5 mags optical flaring event in the FU Ori-like object V1057 Cyg that begun in 1969 (Herbig, 1977). The 1720 MHz OH maser was firstly detected by Lo & Bechis, (1973) and its intensity drastically reduced exponentially over a period of two years beyond detection (Andersson, *et al.*, 1979). Another significant OH outburst was detected in 1979 which drastically reduced by a factor of two within two months (Winnberg *et al.*, 1981). A similar behavior was observed in some features of methanol maser associated NGC 6334I in which a rapid flare was noticed followed by a rapid decline within the same time scale (MacLeod *et al.*, 2018). However, this is not the case for the 1665 MHz OH maser whose flux remained high for some features.

MacLeod *et al.*, (2018) suggests an alternative hypothesis to explain the observed flaring in Kitty which concerns high energy produced from a supernova that causes dust in the surrounding regions to heat up hence radiatively pumping the masers. Also associated with supernova blasts are ejectas that may produce non thermal emissions such as those from CM2 2'' north of MM1 which were already listed in the VLA observations of 2011. However, embedded supernova are usually associated with new and strong centimeter continuum emissions which have not been observed anywhere near our flaring sources. As a result, this rules out the possibility of a supernova to have caused the observed outburst.

5.4 Magnetic Field in NGC 6334I

Magnetic field determination in the past studies has used data from VLBI observations which normally have high resolution (Fish *et al.*, 2003). Using data from a single dish observation such as the 26 m HartRAO radio telescope, it was only possible to approximate the magnetic field in star forming regions by means of identifying Zeeman pairs. Therefore, the magnetic field determined using this approach was found to be $-5.8 \text{ mG} \pm 0.5 \text{ mG}$. This means that the magnetic field is oriented towards our line of sight.

The implication of this magnetic field in this star forming region is that it caused OH and other molecules that produce masers to become circularly and linearly polarized. On the other hand, the magnetic field in star forming regions are responsible for causing masing molecules and other maser sources to split and hence produce Zeeman pairs.

Fish *et al.*, (2003) reported a magnetic field strength ranging from -5.3 mG in the 1665 MHz transition of the OH maser associated with this region. The orientation of magnetic field agrees well with that reported by Fish *et al.*, (2003). The value reported by Fish is in agreement with our findings at 1665 MHz OH transition.

Considering the angular separation for maser having the velocity -10.6 km s^{-1} in LCP and -6.7 km s^{-1} in RCP which are almost the same (see table 2 and 3), these velocity value could be a Zeeman pair because they showed similar variability in both velocity and flux density. Assuming they are Zeeman pairs, the value of the magnetic field for this region would be $6.61 \pm 0.8 \text{ mG}$ for NGC 6334-V also known as G351.162+0.695. This suggest that the source has a characteristic magnetic field oriented away from the observer. The magnetic field strength values reported by Fish *et al.*, (2003) for this source measured in the 1665 MHz OH maser transition do not exist. However, the value of the magnetic field for this source reported by Fish *et al.*, (2003) was measured in the 1667 MHz OH masers and was 0.2 mG (see Appendix A3). From this value, we can see that the orientation of the magnetic field is the same except for the magnitude. This may suggest that over the years the magnetic field has increased and the increase could be attributed to the recent flaring event reported by MacLeod *et al.*, (2018).

The value of the magnetic field calculated for the source NGC 6334I differs in orientation from that calculated for NGC 6334-V simply because the two maser sources are different. However, the magnitudes for their magnetic field are within the same error and show an increase compared to the previously reported values (see Appendix A3). This suggests that the magnetic field orientation in star-forming regions are not uniform but are localized which

agrees well with the findings by Fish *et al.*, (2003).

6 CONCLUSION AND RECOMMENDATIONS

6.1 Conclusion

The period of variation in the peak velocity of the 1665 MHz OH masers associated with NGC 6334I was found to be 366.01 ± 3.33 , and 365.89 ± 1.28 in the LCP, and 366.69 ± 1.38 days in the RCP. These maser features were found at -10.6 km s^{-1} and -10.2 km s^{-1} in the LCP, and at -6.7 km s^{-1} in the RCP. The values of the period are within the error of one earth year which suggest that the cause of this variation was uncorrected earth's motion for these features during observation. The maser source that caused this variability was identified as NGC 6334-V located South of NGC 6334I. The maser source NGC 6334-V was far enough from the beam center of the telescope such that the V_{lsr} employed during observations for NGC 6334I were not correct for NGC 6334-V

The maser features that showed periodic variation in peak velocity showed an antagonistic change in flux density. The flux of maser features in the LCP with peak velocity -10.2 km s^{-1} showed a gradual increase in flux with time while that of the RCP with peak velocity of -6.7 km s^{-1} showed a rapid decrease in flux. Another form of variation observed was in the flux density of selected maser spectra positioned at -7.92 and -8.19 km s^{-1} in the LCP and -7.40 and -7.22 km s^{-1} in the RCP. These masers showed increased flux from around August 14, 2015, to December 16, 2016, when the last observation included here was done. The causes of the increased flux density (flaring) are not very clear. However, one viable explanation is that it was caused by an accretion event that occurred in a low mass star forming region close to NGC 6334I which supplied extra infrared photons which in turn radiatively pumped the masers.

The star-forming regions NGC 6334I and NGC 6334-V are characterized by a magnetic field of $-5.8 \pm 0.3 \text{ mG}$ oriented towards our line of sight and $6.61 \pm 0.8 \text{ mG}$ away from our line of sight respectively. The difference in the magnitude and orientation of the magnetic field strength suggests that magnetic field strength in star forming regions is localized.

6.2 Recommendations

Future 1665 MHz OH maser observations of NGC 6334I at HartRAO can consider applying V_{lsr} for NGC 6334-V in order to prevent maser features from this source causing periodic variations in peak velocity. In line with this, we recommend the development of an algo-

rithm that will be able to automatically remove interfering maser sources during the data processing.

Since the data used in determining the magnetic field is from a single dish observation, I recommend that VLBI experiments be conducted in order to map the magnetic field strength in the region and determine if the magnetic field strength changed during the flaring. I also suggest that VLBI experiments be conducted to determine the exact locations of the 1665 MHz OH masers whose V_{lsr} were not corrected so that in future observations their V_{lsr} could be considered during observation and hence be corrected.

APPENDIX A1

1. The level of splitting is given by equation 1, which is

$$\Delta v_z = g\mu_0\mathbf{B}/h = b\mathbf{B}/2$$

and equation 6 gives us a relationship between the magnetic field \mathbf{B} and the difference in the Stokes V parameters as shown.

$$\mathbf{B}[mG] = f(V_{RCP} - V_{LCP})$$

we make \mathbf{B} the subject of the formula

$$\mathbf{B} = 2\Delta V_z/b = f(V_{RCP} - V_{LCP})$$

APPENDIX A2

Period04- brief write up Period04 is a computer program that runs on both windows and Linux Operating Systems. The program is especially designed and dedicated to the statistical analysis of large astronomical time series containing gaps. The program contains a number of tools that can be used to extract the individual frequencies from multi-periodic content of time series and it provides a flexible interface to perform multiple frequency fits. To achieve all this, the program has 3 main modules which it uses:

1. The time series Module: This module allows the user to load the time string data into the program. It also allows the user to split or combine data sets, set weights etc.
2. Fit module: This module allows the user to perform least square fits of a number of different frequencies. It also allows the user to fit amplitude, phase variation or take into account a periodic time shift. The fit module contains tools for calculating uncertainties of fit parameters, such as Monte Carlo Simulation.
3. The Fourier Module: This module allows the user to extract new frequencies from the data. It achieves this by using Direct Fourier Transform (DFT) and Fast Fourier Transform (FFT) algorithm because astronomical data is usually not equally spaced.

APPENDIX A3

The following are the scripts that were used in the data reduction and processing:

reduce_1pr

```
# first manually delete any .fits files that are not part of matched pairs

# convert .fits data files to .csv for Lines
sy spfits2asc *.fits
# remove any existing list of csv files
sy rm nextfile
# create a list of files to read in, in a file called 'nextfile':
sy ls *.csv > nextfile
# remove any existing output files (in case it is rerun
sy rm lcp_k.asc
sy rm rcp_k.asc
# set screen plot device as xwindows
set plotdev /xw

#
# read first pair of bandpasses, combine to create spectra, save to disk
# read in nccs csv bandpass 1 from first file listed in nextfile
rncsv nextfile
# copy lcp bandpass to memory 1, rcp bandpass to memory 2
cp 12 1

textttcp 13 2
# plot bandpasses
set colour 2
pl 1
pause
set colour 3
pl 2
pause
```

```

# read in nccs csv bandpass 2
rncsv nextfile
# copy lcp bandpass to memory 3, rcp bandpass to memory 4
cp 12 3

textttcp 13 4
# plot bandpasses
set colour 2
pl 3
pause
set colour 3
pl 4
pause
# combine the lcp bandpasses to produce the lcp spectrum in memory 5
cmb 1 3 5
set colour 2
pl 5
pause
# combine the rcp bandpasses to produce the rcp spectrum in memory 5
cmb 2 4 6
set colour 3
pl 6
pause
# write out the lcp spectrum in ascii file format for easy adding
wa lcp_k.asc 5
# write out the rcp spectrum in ascii file format for easy adding
wa rcp_k.asc 6

end

# close nextfile
nfclose
# clear memories
clr all

```

reduce_2pr

first manually delete any .fits files that are not part of matched pairs

```
# # convert .fits data files to .csv for Lines
```

```
sy spfits2asc *.fits
```

```
# remove any existing list of csv files
```

```
sy rm nextfile
```

```
# create a list of files to read in, in a file called 'nextfile':
```

```
sy ls *.csv > nextfile # remove any existing output files (in case it is rerun)
```

```
sy rm lcp_k.asc
```

```
sy rm rcp_k.asc
```

```
# set screen plot device as xwindows
```

```
set plotdev /xw
```

```
# read first pair of bandpasses, combine to create spectra, save to disk
```

```
# read in nccs csv bandpass 1 from first file listed in nextfile
```

```
rncsv nextfile # copy lcp bandpass to memory 1, rcp bandpass to memory 2
```

```
cp 12 1 cp 13 2 # plot bandpasses
```

```
set colour 2
```

```
pl 1
```

```
pause
```

```
set colour 3
```

```
pl 2
```

```
pause
```

```
# read in nccs csv bandpass 2
```

```
rncsv nextfile
```

```
# copy lcp bandpass to memory 3, rcp bandpass to memory 4
```

```
cp 12 3
```

```
cp 13 4
```

```
# plot bandpasses
```

```
set colour 2
```

```
pl 3
```

```
pause
```

```
set colour 3
```

```

p1 4
pause
# combine the lcp bandpasses to produce the lcp spectrum in memory 5
cmb 1 3 5
set colour 2
p1 5
pause # combine the rcp bandpasses to produce the rcp spectrum in memory 5
cmb 2 4 6
set colour 3
p1 6
pause
# write out the lcp spectrum in ascii file format for easy adding
wa lcp_k.asc 5
# write out the rcp spectrum in ascii file format for easy adding
wa rcp_k.asc 6

#####

# read second pair of bandpasses, combine to create spectra, save to disk
# read in nccs csv bandpass 1 from first file listed in nextfile
rncsv nextfile
# copy lcp bandpass to memory 1, rcp bandpass to memory 2
cp 12 1
cp 13 2
# plot bandpasses
set colour 2
p1 1
pause
set colour 3
p1 2
pause
# read in nccs csv bandpass 2
rncsv nextfile
# copy lcp bandpass to memory 3, rcp bandpass to memory 4

```

```
cp 12 3 cp 13 4 # plot bandpasses
set colour 2
pl 3
pause
set colour 3
pl 4
pause
# combine the lcp bandpasses to produce the lcp spectrum in memory 5
cmb 1 3 5
set colour 2
pl 5
pause
# combine the rcp bandpasses to produce the rcp spectrum in memory 5
cmb 2 4 6
set colour 3
pl 6
pause
# write out the lcp spectrum in ascii file format for easy adding
wa lcp_k.asc 5
# write out the rcp spectrum in ascii file format for easy adding
wa rcp_k.asc 6
end

#
# close nextfile
nfclose
# clear memories
clr all
```

Script for the analysis of the flaring event in NGC 6334I which was run in jupyter notebook.

```
import os
import matplotlib.pyplot as plt
import numpy as np
from astropy.time import Time
#import mpld3 interactive plots
from matplotlib.ticker import MaxNLocator

def load_spectra(filename):
data = np.genfromtxt(filename, delimiter = ',', dtype='float', skip_header=1, unpack=True)
n_vels = data.shape[1]
n_obs = data.shape[0]
#unpack the data
# First row is velocity, with first element a placeholder.
vel = data[0][range(1,n_vels)]
# first column is time, with the same first element as a placeholder
mjd = Time(np.transpose(data)[0][range(1,n_obs)]+49999.5-50000, format='mjd')
temp = data[range(1,n_obs)]
spectra = temp.transpose()[range(1,n_vels)]
#Generating lots of eps files takes a long time if the notebook has just been started up.
#if we just want to recalculate something and don't need to regenerate all the plots set this
to false
make_eps = False

from matplotlib import rc
rc('font', **'family': 'sans-serif', 'sans-serif': ['Helvetica'])
rc('text', usetex=True)
rc('font', size=15)
from matplotlib.ticker import MaxNLocator
```

```
def eps_fix_bbox(fname):
"""Fix the bounding box of an eps file by running ps2eps on it. If its name ends in .eps, the
original file is removed. This is particularly useful for plots made by Gnuplot with square
```

```

aspect ratio: there is a bug in Gnuplot which makes it generate a bounding box which is far
wider than the actual plot. This function assumes that ps2eps is installed in your system.""
# note: ps2ps and eps2eps do NOT work, ONLY ps2eps works correctly. The # others make
output with bitmapped fonts, which looks horrible. print 'Fixing eps file: <os.system('ps2eps
-f -q -l if fname.endswith('.eps'):
os.rename(fname + '.eps', fname)
os.chdir(r'/Users/hp/Desktop/work')

    tick_dates = Time(['2012-01-01',
'2013-01-01',
'2014-01-01',
'2015-01-01',
'2016-01-01',
'2017-01-01'], out_subfmt='date')
ticks = tick_dates.mjd-50000
labels = tick_dates.iso
labels = '2012', '2013', '2014', '2015', '2016', '2017'
X_1665_lcp, Y_1665_lcp = np.meshgrid(mjd_1665_lcp.mjd, vels_1665_lcp)

    fig = plt.figure(figsize=[20, 10], dpi=300)
ax1 = plt.subplot(111)
cax = ax1.pcolormesh(X_1665_lcp, Y_1665_lcp, spectra_1665_lcp, vmin=0, vmax=500, cmap='Spectral')
cbar = fig.colorbar(cax)
cbar.set_label('Flux Density [Jy]', fontname='sans-serif', fontsize=30)

    TickS = 0,50,100,150,200,250,300,350,400,450,500
LabelS = '0', ',', '100', ',', '200', ',', '300', ',', '400', ',', '500

    cbar.set_ticks(TickS)
cbar.ax.tick_params(labelsize=30)
cbar.set_ticklabels(LabelS)

    ax1.set_ylabel('Vlsr [km
s-1]', fontname='sans-serif', fontsize=30)

```

```

ax1.set_xlabel("MJD (+50000)",fontname='sans-serif',fontsize=30) plt.axis('tight')

#change color and linewidth of axis
for axis in ['top','bottom','left','right']:
ax1.spines[axis].set_linewidth(2.0)
ax1.spines[axis].set_color("k")

#set tick sizes
ax1.xaxis.set_tick_params(length=7.5)
ax1.yaxis.set_tick_params(length=7.5)

ax1.xaxis.set_tick_params(width=2)
ax1.yaxis.set_tick_params(width=2)

ticksx=6000,6250,6500,6750,7000,7250,7500,7750,
labelsx='6000',' ',' ','7000',' ',' ','8000'
plt.xticks(ticksx, labelsx, fontname='sans-serif', fontsize=30)

ticksy=-13,-12,-11,-10,-9,-8,-7,-6
labelsy="','-12',' ','-10',' ','-8',' ','-6'
plt.yticks(ticksy, labelsy, fontname='sans-serif', fontsize=30)

#add text
txt1 = '1.665 GHz OH'

ax1.text(5900, -6.50, txt1, fontname='sans-serif', fontsize=30, color='red')

#Make a dummy axis to put dates on top
ax2 = plt.twinx(ax1)
ax2.set_xlim(ax1.get_xlim())

#set tick sizes
ax2.xaxis.set_tick_params(length=7.5)
ax2.xaxis.set_tick_params(width=2)

```



```
labels = '2012', '2013', '2014', '2015', '2016', '2017'  
plt.xticks(ticks, labels, rotation=0, fontsize=30)
```

```
#add a vertical line  
xx = [7023.5, 7023.5]  
yy = [-100, 20000]  
plt.plot(xx, yy, '-b',linewidth=3.0)
```

```
#add a vertical line  
xx = [7249.5, 7249.5]  
yy = [-100, 20000]  
plt.plot(xx, yy, '-k',linewidth=3.0)
```

```
#add a vertical line - 2yrs after Kitty on 1-Sep-17  
xx = [7998, 7998]  
yy = [-100, 20000]  
plt.plot(xx, yy, '-r',linewidth=3.0)
```

```
#change MJD range to plot here  
plt.xlim(5856.161,7734.848)
```

```
#change velocity range to plot here  
plt.ylim(-12,-6)
```

```
plt.savefig('1665_cont.png', bbox_inches='tight')  
plt.plot(vels_1665_lcp, np.mean(spectra_1665_lcp, axis=1))  
plt.plot(vels_1665_lcp, np.max(spectra_1665_lcp, axis=1))  
plt.plot(vels_1665_lcp, np.min(spectra_1665_lcp, axis=1))  
plt.xlim(-20, 5)  
plt.savefig('1665_max.png', bbox_inches='tight')
```

```
def load_spectra1(filename):  
data1 = np.genfromtxt(filename, delimiter = ',', dtype='float', skip_header=1, unpack=True,
```

```

invalid_raise=False, comments=None )
n_vels1 = data1.shape[1]
n_obs1 = data1.shape[0]
#unpack the data
# First row is velocity, with first element a placeholder.
vel1 = data1[0][range(1,n_vels1)]
# first column is time, with the same first element as a placeholder
mjd1 = Time(np.transpose(data1)[0][range(1,n_obs1)]+49999.5-50000, format='mjd')
temp1 = data1[range(1,n_obs1)]
spectra1 = temp1.transpose()[range(1,n_vels1)]
return mjd1, vel1, spectra1

filename = 'oh1665R2018.csv'
data1 = np.genfromtxt(filename, dtype=float, delimiter = ',', skip_header=1, unpack=True,
usecols=np.arange(0,207), comments=None )
mjd_1665_rcp = Time(data1[1:,0]+49999.5-50000, format= 'mjd')
vels_1665_rcp = data1[0,1:]
spectra_1665_rcp = np.transpose(data1[1:,1:])

mjd_1665_rcp, vels_1665_rcp, spectra_1665_rcp = load_spectral1(filename)

#reshape x and y axes for grid plotting.
X_1665_rcp, Y_1665_rcp = np.meshgrid(mjd_1665_rcp.mjd, vels_1665_rcp)

height = 10
width = 10
fig = plt.figure(figsize=[width,height])
#plt.subplots_adjust(hspace=0.35, right=1.0)

#tile 1 - all 1665 LCP data
ax1 = plt.subplot(2,1,1)
cax = ax1.pcolormesh(X_1665_lcp,Y_1665_lcp, spectra_1665_lcp, vmin=-10, vmax=600,
cmap='Spectral_r')
cbar = fig.colorbar(cax)

```

```

cbar.set_label('Flux Density [Jy]', fontsize=20)
ax1.set_ylabel(r"$V_{lsr}$ (km s$^{-1}$)", fontsize=20)
#ax1.set_xlabel("MJD")
#ax1.set_xticklabels([])
plt.axis('tight')
plt.setp(ax1.get_xticklabels(), visible=False)
plt.setp(ax1.get_yticklabels(), fontsize=20)

```

```

#add a vertical line
xx = [7023.5, 7023.5]
yy = [-100, 100]
plt.plot(xx, yy, '-k')

```

```

#add a vertical line
xx = [7249.5, 7249.5]
yy = [-100, 100]
plt.plot(xx, yy, '-k')

```

```

#add text
txt1 = '(a) LCP'
ax1.text(5900, -6.7, txt1, fontsize=20)

```

```

#change MJD range to plot here
plt.xlim(5856.161,7734.848)

```

```

#change velocity range to plot here
plt.ylim(-14,-6)

```

```

#Make a dummy axis to put dates on top
ax3 = plt.twinx(ax1)
ax3.set_xlim(ax1.get_xlim())
labels = '2012', '2013', '2014', '2015', '2016', '2017'
plt.xticks(ticks, labels, fontsize=20)

```

```

#tile 2 - all 1665 RCP data
ax2 = plt.subplot(212)
cax = ax2.pcolormesh(X_1665_rcp,Y_1665_rcp, spectra_1665_rcp, vmin=-10, vmax=130,
cmap='Spectral_r')
cbar = fig.colorbar(cax)
cbar.set_label('Flux Density [Jy]', fontsize=20)
ax2.set_ylabel(r" $V_{lsr}$  (km s-1)", fontsize=20)
ax2.set_xlabel("MJD (+50 000)", fontsize=20)
plt.axis('tight')
plt.setp(ax2.get_xticklabels(), fontsize=18)
plt.setp(ax2.get_yticklabels(), fontsize=20)

#add a vertical line
xx = [7023.5, 7023.5]
yy = [-100, 100]
plt.plot(xx, yy, '-k')

#add a vertical line
xx = [7249.5, 7249.5]
yy = [-100, 100]
plt.plot(xx, yy, '-k')

#add text
txt2 = '(b) RCP'
ax2.text(5900, -13.7, txt2, fontsize=20)

#change MJD range to plot here
plt.xlim(5856.161,7734.848)

#change velocity range to plot here
plt.ylim(-14,-6)

#Make a dummy axis to put dates on top
ax4 = plt.twinx(ax2)

```

```

ax4.set_xlim(ax2.get_xlim())
labels = ",,,"
plt.xticks(ticks, labels)

plt.savefig('oh1665_ct.png', bbox_inches='tight')
make_eps = True
if make_eps:
outfile = 'fig13_1665ct.eps'
plt.savefig(outfile, format='eps')

height = 10
width = 10
fig = plt.figure(figsize=[width,height])
#plt.subplots_adjust(hspace=0.35, right=1.0)

#tile 1 - all 1665 LCP data
ax1 = plt.subplot(2,1,1)
cax = ax1.pcolormesh(X_1665_lcp,Y_1665_lcp, spectra_1665_lcp, vmin=-10, vmax=600,
cmap='Spectral_r')
cbar = fig.colorbar(cax)
cbar.set_label('Flux Density [Jy]', fontsize=28)
ax1.set_ylabel(r" $V_{lsr}$  [km s-1]", fontsize=28)
#ax1.set_xlabel("MJD")
ax1.set_xticklabels([])
plt.axis('tight')

plt.setp(ax1.get_yticklabels(), fontsize=20)

#add a vertical line
xx = [7023.5, 7023.5]
yy = [-100, 100]
plt.plot(xx, yy, '-k')

#add a vertical line

```

```

xx = [7249.5, 7249.5]
yy = [-100, 100]
plt.plot(xx, yy, '-k')

#add text
txt1 = '1665 MHz OH LCP'
ax1.text(5900, -1.5, txt1, fontsize=28)

#change MJD range to plot here
plt.xlim(5856.161,7991.217)

#change velocity range to plot here
plt.ylim(-15,0)

#Make a dummy axis to put dates on top
ax3 = plt.twinx(ax1)
ax3.set_xlim(ax1.get_xlim())
labels = '2012','2013','2014','2015','2016','2017'
plt.xticks(ticks, labels, fontsize=20)

#tile 2 - all 1665 RCP data
ax2 = plt.subplot(212)
cax = ax2.pcolormesh(X_1665_rcp,Y_1665_rcp, spectra_1665_rcp, vmin=-10, vmax=130,
cmap='Spectral_r')
cbar = fig.colorbar(cax)
cbar.set_label('Flux Density [Jy]', fontsize=28)
ax2.set_ylabel(r" $V_{lsr}$  [km s-1]", fontsize=28)
ax2.set_xlabel("MJD", fontsize=28)
plt.axis('tight')

plt.setp(ax2.get_xticklabels(), fontsize=20)
plt.setp(ax2.get_yticklabels(), fontsize=20)

#add a vertical line

```



```

width = 14
fig = plt.figure(figsize=[width,height])
#plt.subplots_adjust(hspace=0.0, right=0.85)

#tile 1 - 1665 LCP time-series components associated with Kitty
ax1 = plt.subplot(222)

vel, idx = find_nearest(vels_1665_lcp, -7.62)
plt.plot(mjd_1665_lcp.mjd, spectra_1665_lcp[idx], 'cs', label=np.str(np.round(vel,2)))
vel, idx = find_nearest(vels_1665_lcp, -7.92)
plt.plot(mjd_1665_lcp.mjd, spectra_1665_lcp[idx], 'bs', label=np.str(np.round(vel,2)))
vel, idx = find_nearest(vels_1665_lcp, -8.2)
plt.plot(mjd_1665_lcp.mjd, spectra_1665_lcp[idx], 'ro', label=np.str(np.round(vel,2)))
vel, idx = find_nearest(vels_1665_lcp, -8.45)
plt.plot(mjd_1665_lcp.mjd, spectra_1665_lcp[idx], 'gd', label=np.str(np.round(vel,2)))
vel, idx = find_nearest(vels_1665_lcp, -9.68)
plt.plot(mjd_1665_lcp.mjd, spectra_1665_lcp[idx], 'c', label=np.str(np.round(vel,2)))

plt.legend(bbox_to_anchor=(.485, 1.01), fontsize=20, handlelength=0.75, columnspacing=0.01, handletextpad=0.5, borderpad=0.1, numpoints=1, loc=1)
plt.axis('tight')
ax1.set_xticklabels([])
#ax1.set_yticklabels([])

#ax1.set_ylabel('Flux density (Jy)')
#plt.setp(ax1.get_xticklabels(), fontsize=20)
plt.setp(ax1.get_yticklabels(), fontsize=20)

#add a vertical line
xx = [7023.5, 7023.5]
yy = [-100, 20000]
plt.plot(xx, yy, '-k')

#add a vertical line

```



```

xx = [7239.5, 7239.5]
yy = [-100, 20000]
plt.plot(xx, yy, '-k')

    #add a horizontal line
xx = [5000, 9000]
yy = [0, 0]
plt.plot(xx, yy, '-k', linewidth=0.75)

    #add text
txt1 = '(b) LCP'
ax1.text(5950, 190, txt1, fontsize=20)

    #change MJD and Flux range to plot here
plt.xlim(5856.161,8114.905)
plt.ylim(-10, 211)

    #Make a dummy axis to put dates on top
ax5 = plt.twinx(ax1)
ax5.set_xlim(ax1.get_xlim())
labels = '2012', '2013', '2014', '2015', '2016', '2017'
plt.xticks(ticks, labels, fontsize=20)

    #tile 2 - 1665 LCP spectra before, during and after Kitty
ax2 = plt.subplot(221)

    #select idx=125 = 10-Jan-15 before Kitty
yy = spectra_1665_lcp[:,125]
plt.plot(vels_1665_lcp, yy, '-b', label='10 Jan 15')

    #select idx=141 = 11-Sep-15 during Kitty
yy = spectra_1665_lcp[:,141]
plt.plot(vels_1665_lcp, yy, '-k', label='11 Sep 15')

```

```

#select idx=228 = 25-Aug-17 after Kitty
yy = spectra_1665_lcp[:,205]
plt.plot(vels_1665_lcp, yy, '-r', label='25 Aug 16')

plt.legend(bbox_to_anchor=(.95, 1), fontsize=20, handlelength=0.75, columnspacing=0.01,
handletextpad=0.5, borderpad=0.2, numpoints=1, loc=1)
ax2.set_ylabel('Flux Density [Jy]', fontsize=20)
#ax2.set_xlabel(r"$V_{lsr}$ (km s$^{-1}$)")
ax2.set_xticklabels([])
plt.axis('tight')
#plt.setp(ax2.get_xticklabels(), fontsize=20)
plt.setp(ax2.get_yticklabels(), fontsize=20)

#was (20,10)
plt.xlim(-20,0)
plt.ylim(-10, 800)

#add a horizontal line
xx = [-50, 50]
yy = [0, 0]
plt.plot(xx, yy, '-k', linewidth=0.75)

#add text
txt2 = '(a) LCP'
ax2.text(-19, 560, txt2, fontsize=20)

#tile 3 - 1665 RCP spectra before, during and after Kitty
ax3 = plt.subplot(224)

vel, idx = find_nearest(vels_1665_rcp, -8.20)
plt.plot(mjd_1665_rcp.mjd, spectra_1665_rcp[idx], 'bs', label=np.str(np.round(vel,2)))
vel, idx = find_nearest(vels_1665_rcp, -7.4)
plt.plot(mjd_1665_rcp.mjd, spectra_1665_rcp[idx], 'ro', label=np.str(np.round(vel,2)))
#vel, idx = find_nearest(vels_1665_rcp, -6.8)

```

```

plt.plot(mjd_1665_rcp.mjd, spectra_1665_rcp[idx], 'gd', label=np.str(np.round(vel,2)))
vel, idx = find_nearest(vels_1665_rcp, -7.2)
plt.plot(mjd_1665_rcp.mjd, spectra_1665_rcp[idx], 'cs', label=np.str(np.round(vel,2)))

    plt.legend(bbox_to_anchor=(.485, 1.01), fontsize=20, handlelength=0.75, columnspac-
ing=0.01, handletextpad=0.5, borderpad=0.2, numpoints=1, loc=1)
plt.axis('tight')
#ax3.set_ylabel('Flux density (Jy)')
ax3.set_xlabel("MJD (+50 000)", fontsize=20)
plt.setp(ax3.get_xticklabels(), fontsize=20)
plt.setp(ax3.get_yticklabels(), fontsize=20)

    #add a vertical line
xx = [7023.5, 7023.5]
yy = [-100, 20000]
plt.plot(xx, yy, '-k')

    #add a vertical line
xx = [7239.5, 7239.5]
yy = [-100, 20000]
plt.plot(xx, yy, '-k')

    #add a horizontal line
xx = [5000, 9000]
yy = [0, 0]
plt.plot(xx, yy, '-k', linewidth=0.75)

    #add text
txt3 = '(d) RCP'
ax3.text(5950, 65, txt3, fontsize=20)

    #change MJD range to plot here
plt.xlim(5856.161,8114.905)
plt.ylim(-10, 70)

```

```

#Make a dummy axis to put dates on top
ax6 = plt.twinx(ax3)
ax6.set_xlim(ax3.get_xlim())
#labels = '2012', '2013', '2014', '2015', '2016', '2017'
labels = ",, ,, , , "
plt.xticks(ticks, labels)

#tile 4 - 1665 RCP time-series components associated with Kitty
ax4 = plt.subplot(223)

#select idx=125 = 10-Jan-15 before Kitty
yy = spectra_1665_rcp[:,125]
plt.plot(vels_1665_rcp, yy, '-b', label='10 Jan 15')

#select idx=141 = 11-Sep-15 during Kitty
yy = spectra_1665_rcp[:,141]
plt.plot(vels_1665_rcp, yy, '-k', label='11 Sep 15')

#select idx=209 = 25-feb-17 after
yy = spectra_1665_rcp[:,205]
plt.plot(vels_1665rcp, yy, '-r', label='25 Aug 16')

plt.legend(bbox_to_anchor=(.95, 1), fontsize=20, handlelength=0.75, columnspacing=0.01,
handletextpad=0.5, borderpad=0.2, numpoints=1, loc=1)
ax4.set_ylabel('Flux Density [Jy]', fontsize=20)
ax4.set_xlabel(r" $V_{lsr}$  [km s-1]", fontsize=20)
plt.axis('tight')
plt.setp(ax4.get_xticklabels(), fontsize=20)
plt.setp(ax4.get_yticklabels(), fontsize=20)

#was (20,10)
plt.xlim(-20, 0)
plt.ylim(-10, 110)

```

```
#add a horizontal line
xx = [-50, 50]
yy = [0, 0]
plt.plot(xx, yy, '-k', linewidth=0.75)

#add text
txt4 = '(c) RCP'
ax4.text(-19, 103, txt4, fontsize=20)

#save images as png and eps
plt.savefig('oh1665_ts.png', bbox_inches='tight')
```

APPENDIX A4

Zeeman pairs and magnetic field survey by Fish *et al.*,(2003). NOTE NGC 6334I corresponds to G351.416+0.646

Table 1—Continued

Source	Alias	Dist. ^a (kpc)	Freq. (MHz)	-LCP			-RCP			$\Delta\theta^c$ (arcsec)	B^d (mG)	Grade ^e
				S^b (Jy)	v_{LSR}^b (km s ⁻¹)	Δv^b (km s ⁻¹)	S^b (Jy)	v_{LSR}^b (km s ⁻¹)	Δv^b (km s ⁻¹)			
G213.706-12.60	Mon R2	0.9	1665	0.12	12.36	0.46	0.62	10.37	0.38	0.067	-3.4	B
G341.219-0.212	...	3.2	1665	3.49	-40.85	0.45	10.06	-37.40	0.33	0.027	5.8	B
G343.128-0.063	...	3.1	1665	86.65	-31.74	0.38	13.64	-30.69	0.33	0.024	1.8→5.5	C
G344.581-0.022	...	0.6	1665	0.82	0.90	0.60	0.57	-0.78	0.80	0.046	-2.8	B
				2.23	-4.40	0.69	18.57	-2.33	0.58	0.060	0.7→3.9	C
				14.33	-2.62	0.68	0.85	1.34	0.34	0.110	4.2→6.7	C
G345.003-0.224	...	2.9	1720	52.64	-29.24	0.33	2.16	-28.80	0.44	0.008	1.9	B
G345.011+1.792	...	2.2	1665	0.68	-18.99	0.27	20.22	-20.44	0.41	0.083	-2.5	B
				30.84	-22.74	0.37	10.32	-19.72	0.25	0.105	3.3→5.1	C
G345.505+0.347	...	2.1	1665	10.91	-17.32	0.35	4.37	-18.01	0.27	0.106	-1.2→-1.8	C
			1667	2.37	-12.74	0.35	4.98	-12.69	0.32	0.013	0.1	B
				1.15	-21.58	0.37	3.78	-21.25	0.31	0.011	0.9	B
G345.699-0.090	...	1.6	1665	0.52	-8.47	0.29	3.58	-8.22	0.22	0.091	0.4	B
G347.628+0.149	...	9.8	1612	3.02	-97.16	0.27	5.89	-96.42	0.27	0.014	3.1	B
G348.549-0.978	...	2.2	1665	2.72	-19.87	0.46	6.52	-19.84	0.44	0.040	0.1→11.5	C
			1720	4.74	-12.77	0.36	4.49	-13.38	0.38	0.036	-2.6	B
G350.011-1.341	...	3.1	1665	5.33	-19.74	0.29	3.56	-19.32	0.24	0.023	0.7	B
G351.161+0.697	NGC 6334 B	2.3	1667	20.11	-9.72	0.32	78.79	-9.64	0.22	0.028	0.2	B
				7.37	-15.29	0.29	5.08	-15.24	0.30	0.006	0.1	B
G351.416+0.646	NGC 6334 F	2.0	1665	184.98	-8.87	0.32	31.40	-11.99	0.57	0.045	-5.3	B
			1667	47.77	-9.26	0.27	54.05	-11.11	0.28	0.022	-2.2→-5.2	C
			1720	84.48	-9.84	0.32	61.20	-10.58	0.34	0.020	-3.1	B
G351.582-0.352	...	6.7	1665	2.73	-90.97	0.32	5.82	-93.87	0.25	0.019	-4.9	B
G351.775-0.538	...	2.7	1665	2.94	-25.62	0.46	4.80	-27.86	0.39	0.025	-3.8	A
				777.34	-1.95	0.40	106.28	-1.85	0.47	0.013	0.2	B
				4.09	-8.04	0.29	6.92	-7.84	1.06	0.063	0.3	B
				54.35	-6.88	0.40	4.42	-10.16	0.57	0.047	-5.6→-6.5	C
			1667	3.06	-26.15	0.43	4.23	-27.44	0.44	0.014	-3.7	A
				58.40	-6.97	0.30	1.85	-4.95	0.38	0.029	5.7	B
				10.02	-5.55	0.27	2.62	-5.83	0.29	0.024	-0.8	B
				1.51	0.37	0.42	1.49	-0.16	0.67	0.037	-0.3→-1.5	C
G353.410-0.361	...	3.8	1665	19.83	-19.56	0.29	3.30	-19.50	0.48	0.033	0.1→2.4	C
G355.345+0.146	...	23.1	1665	17.07	19.71	0.42	15.34	16.54	0.86	0.006	-3.4→-5.4	C
G359.138+0.032	...	3.1	1665	4.60	-0.21	0.40	3.32	-2.98	0.71	0.014	-4.7	B
				2.92	-6.20	0.37	1.39	-6.09	0.31	0.047	0.2	B

Figure 13: Zeeman pairs and magnetic field studies conducted by Fish *et al.*, 2003

APPENDIX A5

Two papers have been published containing results of this research. The titles and the Abstracts are included here.

A Masing Event in NGC 6334I: Contemporaneous Flaring of Hydroxyl, Methanol and Water Masers

G. C. MacLeod^{1*}, D. P. Smits², S. Goedhart³, T. R. Hunter⁴, C. L. Brogan⁴, J. O. Chibueze^{3,5,6}, S. P. van den Heever¹, C. J. Thesner⁵, P. J. Banda⁷, and J. D. Paulsen⁸

¹Hartebeesthoek Radio Astronomy Observatory, PO Box 443, Krugersdorp, 1741, South Africa

²Dept of Mathematical Sciences, UNISA, PO Box 392, UNISA, 0003, South Africa

³SKA SA, The Park, Park Road, Pinelands, South Africa

⁴NRAO, 520 Edgemont Rd, Charlottesville, VA, 22903, USA

⁵Space Research Unit, Physics Department, North West University, Potchefstroom, South Africa

⁶Department of Physics and Astronomy, University of Nigeria, Carver Building, 1 University Road, Nsukka, Nigeria

⁷School of Physical Sciences, University of Nairobi, Nairobi, Kenya

⁸Trinity House High School, Little Falls, South Africa

Accepted 2018 April 4. Received 2018 March 22; in original form 2017 October 18

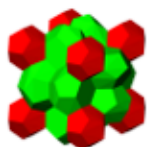
ABSTRACT

As a product of the maser monitoring program with the 26 m telescope of the Hartebeesthoek Radio Astronomy Observatory (HartRAO), we present an unprecedented, contemporaneous flaring event of 10 maser transitions in hydroxyl, methanol, and water that began in 2015 January in the massive star-forming region NGC 6334I in the velocity range -10 to -2 km s⁻¹. The 6.7 GHz methanol and 22.2 GHz water masers began flaring within 22 days of each other, while the 12.2 GHz methanol and 1665 MHz hydroxyl masers flared 80 and 113 days later respectively. The 1665 MHz, 6.7 GHz, and 22.2 GHz masers have all remained in their flared state for nearly 3 years. The brightest flaring components increased by factors of 66, 21, 26, and 20 in the 12.2 and 6.7 GHz methanol, 1665 MHz hydroxyl and 22.2 GHz water maser transitions respectively; some weaker components increased by up to a factor of 145. We also report new maser emission in the 1720, 6031, and 6035 MHz OH lines and the 23.1 GHz methanol line, along with the detection of only the fifth 4660 MHz OH maser. We note the correlation of this event with the extraordinary (sub)millimeter continuum outburst from the massive protostellar system NGC 6334I-MM1 and discuss the implications of the observed time lags between different maser velocity components on the nature of the outburst. Finally, we identify two earlier epoch maser flaring events likely associated with this object, which suggest a recurring accretive phenomenon that generates powerful radiative outbursts.

Key words: masers – stars: formation – stars: protostars – radio lines: ISM – ISM: molecules – ISM: individual objects: NGC 6334I

arXiv:1804.05308v1 [astro-ph.SR] 15 Apr 2018

Figure 14: Abstract of a paper that contain some of the results of this thesis which was published in 2018. This paper is available online.



Understanding and Explaining Observed Variability in Microwave Amplification By Stimulated Emission of Radiation (Maser) Sources in NGC 6334 I

P. J. Banda¹, G. O. Okeng'o¹ and G. C. MacLeod²

¹Department of Physics, School of Physical Sciences, College of Biological & Physical Sciences, University of Nairobi, P. O. Box 30197-00100 GPO, Nairobi-Kenya.

²Hartebeesthoek Radio Astronomy Observatory, P. O Box 443, Krugersdorp 1740, Johannesburg, South Africa.

ARTICLE INFO

Available online 00
Month Year

Keywords: Maser,
Star-formation,
Periodic variation

ABSTRACT

Telescopic observations of the star-forming region NGC 6334I, also known as the 'Cats Paw Nebular', has in the recent past shown evidence of periodic variations in the 1665 MHz frequency hydroxyl (OH) masers associated with it. These variations are not only limited to the velocity but also in flux density. This source has been on the ongoing observational program at Hartebeesthoek Radio Astronomy Observatory (Hart RAO) in Johannesburg, South Africa, in order to understand the underlying causes and the associated physics. This work uses five-year data obtained using the Hart RAO 26-meter telescope to determine the period of variability for OH masers in NGC 6334I, as well as compute the magnetic field strengths from Zeeman pairs. It is shown that in the Left Circular Polarization (LCP) the maser variability occurs at -10.5 km/s and -10.2 km/s, with periods of 366.01 ± 3.33 and 365.89 ± 1.28 days respectively. The unprecedented outburst in the flux commenced about 226 days after that which was reported by MacLeod and others and it is also shown that in the LCP the flaring occurred at velocity channels -7.92 km/s and -8.19 km/s in the LCP while in the RCP the flaring occurred at -7.4 km/s and -8.19 km/s

Corresponding author. Tel: +254734458770. E-mail address:
peterjairo6@gmail.com

Figure 15: Abstract of a paper that has been submitted for publication written by Banda *et al.*, 2018

7 LIST OF REFERENCES

- Andersson, C., Johansson, L. E. B., Winnberg, A., Goss, W. M. (1979). *OH observations of V1057 Cyg.*, *A & A*, **80**: 260-264.
- Argon, A. L., Reid, M. J., Menten, K. M. (2000). *Interstellar Hydroxyl Masers in the Galaxy I. The VLA Survey*, **129**:159-227.
- Bally, J., Zinnecker, H. (2005). *The Birth of High-Mass Stars: Accretion and/or Mergers?* , *AJ*, **129**; 2281-2293.
- Clegg, A. W., Cordes, J. M., Simonetti, J. M., Kulkarni, S. R. (1992). *Rotation measures of low-latitude extragalactic sources and the magnetoionic structure of the Galaxy*, *ApJ*, **386**: 143-157.
- Caratti o Garatti, A., Stecklum, B., Garcia Lopez, R., Eislöffel, J., Ray, T. P., Sanna, A., Cesaroni, R., Walmsley, C. M., Oudmaijer, R. D., de Wit, W. J., Moscadelli, L., Greiner, J., Krabbe, A., Fischer, C., Klein, R., Ibañez, J. M. (2017). *Disk-mediated accretion burst in a high-mass young stellar object*, *NatPh*, **13**: 276-279.
- Colom, P., Lekht, E. E., Pashchenko, M. I., Rudnitskii, G. M., Tolmachev, A. M. (2015). *H₂O and OH masers associated with cold infrared sources*, *AstL*, **41**:425-441.
- Cragg, D. M., Sobolev A. M., Godfrey P. D. (2002). *Modelling methanol and hydroxyl masers in star-forming regions* *MNRAS*, **331**: 521
- Crutcher, R. M., Roberts, D. A., Mehringer, D. M., Troland, T. H. (1996). *H i Zeeman Measurements of the Magnetic Field in Sagittarius B2*, *apjl*, **462**:L79.
- Davies, R. D. (1974). *Magnetic Fields in OH Maser Clouds*, *IAU Symp.* **60**: 275.
- De Buizer, J. M. (2002). *The relationship between masers and massive star formation: what can be learned from the infrared ?*, *IAU Symp*, **206**: 18.
- Dickel, H. R. and Goss, W. M. (1987). *VLA observations of the 6 CM and 2 CM lines of H₂CO in the direction of W3(OH)*, *A&A*, **185**: 271-282.
- Elitzur, M. (1992). *Astronomical masers*, *ARA&A*, **30**: 75-112.
- Feigelson., Eric D. (2014). *MYStIX: Massive Young Stellar Cluster Study in Infrared and X-Rays* , Springer, **1**: 485
- Fish, V. L., Reid, M. J. (2006). *Large Magnetic Fields and OH Maser Motions in W75 N*, *AAS*,**209**: 105.18
- Fish, V. L., Reid, M. J. (2006). *Full-Polarization Observations of OH Masers in Massive Star-forming Regions. II. Maser Properties and the Interpretation of Polarization*, *The Astrophysical Journal Supplement Series*,**164**: 99-123

- Fish, V. L., Reid, M. J., Argon, A. L., Menten, K. M. (2003). *Dual Cometary H II Regions in DR 21: Bow Shocks or Champagne Flows?*, *ApJ*, **596**: 328.
- Fish, V. L., Reid, M. J., Menten, K. M., Pillai, T. (2006). *Enhanced density and magnetic fields in interstellar OH masers*, *aap*, **458**:485-495.
- Fukui, Y., Koga, M., Maruyama, S., Okamoto, R., Yamamoto, H., Tachihar, K., Shelton, R., (2017). *An Intermediate Velocity HI Cloud Colliding With The Galactic Disk; Evidence For The Falling HI Gas In The Solar Neighborhood*, *arXiv*, **1711**: 952
- Gray, M. (2012). *Maser Sources in Astrophysics*, Cambridge University Press, Cambridge. pp.10?230
- Gray, M. D., Doel, R. C., Field, D. (1991). *A model for OH masers in star-forming regions*, *MNRAS*, **252**: 30.
- Guesten, R., Fiebig, D. (1990). *Magnetic fields in dark cloud cores and H₂O masers*, *IAU Symposium*, **140**:305-308.
- Habing, H.J., Goss, W. M., Matthews, H. E., Winnberg, A. (1974). *Identification of type I OH masers with very small H II regions*, *aap*, **35**: 1-5.
- Hartmann L., Kenyon S. J. (1996). *The FU Orionis Phenomenon*, *A& A*, **34**: 207-240.
- Harvey, S.L and Cohen, R.J. (2005). *A MERLIN survey of 4.7-GHz excited OH masers in star-forming regions*, *MNRAS* **356**: 637-646.
- Harvey, P. M., Gatley, I. (1983). *Infrared observations of OB star formation in NGC 6334*, *ApJ*, **269**: 613.
- Heiles, C. (1976). *An almost complete survey of 21-centimeter line radiation for galactic latitudes of at least 10 deg. VI - Energetic expanding H I shells*, *ARA&A*, **14**: 1.
- Heiles, C., Goodman, A. A., McKee, C. F., Zweibel, E. G. (1993). *Magnetic fields in star-forming regions - Observations*, *ADS*, **1**:279-326.
- Herbig, G. H. (1977). *Eruptive phenomena in early stellar evolution.* , *AJ*, **217**: 693-715.
- Holtz, J. Z. (1968). *Energy Requirements and Mechanisms for OH Galactic Masers*, *ApJ*, **153**: L117.
- Hunter, T. R., Brogan, C. L., MacLeod, G., Cyganowski, C. J., Chandler, C. J., Chibueze, J. O., Friesen, R., Indebetouw, R., Thesner, C., Young, K. H. (2017). *An Extraordinary Outburst in the Massive Protostellar System NGC6334I-MM1: Quadrupling of the Millimeter Continuum*, preprint, **24**, 2-4.
- Hunter, T. R., Brogan, C. L., Megeath, S. T., Menten, K. M., Beuther, H., Thorwirth, S. (2006). *Millimeter Multiplicity in NGC 6334 I and I(N)*, *Apj*, **647**: 888-893
- Johnstone, D., Hendricks, B., Herczeg, G. J., Bruderer, S. (2013). *Continuum Variability of Deeply Embedded Protostars as a Probe of Envelope Structure*, *Apj*, **765**: 133

- Lo, K. Y., Bechis, K. P. (1973). *Anomalous 1720-MHz OH Emission from V1057 Cygni*, AJ, **185**: L71.
- Kerr, F. J & Simonson, S. C. (1974). *Galactic radio astronomy: proceedings from IAU symposium no. 60 held at Maroochydore Queensland, Australia, 3-7 September, 1973*, IAU Symposium, **60**: 1
- MacLeod, G. C., Gaylard, M. J. (1996). *Variable hydroxyl and methanol masers in G 351.78-0.54*, MNRAS, **280**: 868.
- MacLeod, G. C., Smits, D. P., Goedhart, S., Hunter, T. R., Brogan, C. L., Chibueze, J. O., van den Heever, S. P., Thesner, C. J., Banda, P. J., Paulsen, J. D. (2018). *A masing event in NGC 6334I: contemporaneous flaring of hydroxyl, methanol, and water masers*, MNRAS, **478**: 1077-1092.
- Menten, K.M.,(1991). *The discovery of a new, very strong, and widespread interstellar methanol maser line*, ApJ, **380**, L75.
- Menten, K. M., Batrla, W. (1989). *Observations of various methanol maser transitions toward the NGC 6334 region*, ApJ, **341**, 839.
- Mezger, P. G., Altenhoff, W., Schraml, J., Burke, B.F., Reifenstein, III, E. C., Wilson, T. L. (1967). *A New Class of Compact H II Regions Associated with OH Emission Sources*, ApJ**150**, L157.
- Moran, J. M. (1976). *Very long baseline interferometric observations and data reduction*, MEP, **12**: 385-437.
- Moriarty, C., (2009). *Probing the Magnetic Fields of Star Forming Regions with Methanol Maser Polarisation*, University of Western Australia, Honors thesis.
- Moscadelli, L., Sanna, A., Goddi, C., Walmsley, M. C., Cesaroni, R., Caratti o Garatti, A., Stecklum, B., Menten, K. M., Kraus, A. (2017). *Extended CH₃OH maser flare excited by a bursting massive YSO*, A & A, **600**: L8.
- Neugebauer, G., Leighton, R. B. (1997). *VizieR Online Data Catalog: Two-Micron Sky Survey (TMSS) (Neugebauer+ 1969)*, VizieR Online Data Catalog, **1:II/2B**.
- Persi, P., Tapia, M., Reipurth, B. (2008). *Star Formation in NGC 6334*, ASP, **2**: 456
- Qiao, H.-H., Walsh, A. J., Gómez, J. F., Imai, H., Green, J. A., Dawson, J. R., Shen, Z.-Q., Ellingsen, S.P., Breen, S. L., Jones, P. A., Gibson, S. J., Cunningham, M. R. (2016). *Unusual Shock-excited OH Maser Emission in a Young Planetary Nebula*, apj, **817**: 37.
- Reid, M. J., Moran, J. M., Johnston, K. J. (1981). *Observations of stellar OH masers with the VLA*, AJ, **86**: 897-902.
- Rodriguez, L. F. (1999). *Jets and Outflows from YSOs*, ADS, **1**: 257-262.

Schneider, N., Csengeri, T., Hennemann, M., Motte, F., Didelon, P., Federrath, C., Bontemps, S., Di Francesco, J., Arzoumanian, D., Minier, V., André, Ph., Hill, T., Zavagno, A., Nguyen-Luong, Q., Attard, M., Bernard, J. -Ph., Elia, D., Fallscheer, C., Griffin, M., Kirk, J., Klessen, R., Könyves, V., Martin, P., Men'shchikov, A., Palmeirim, P., Peretto, N., Pestalozzi, M., Russeil, D., Sadavoy, S., Sousbie, T., Testi, L., Tremblin, P., Ward-Thompson, D., White, G. (2013). *Cluster-formation in the Rosette molecular cloud at the junctions of filaments (Corrigendum)*, A&A, **551**: 1.

Spitzer, L., Jr. (1978). *Physical Processes in the Interstellar Medium*, Wiley, New York: pp100

Sullivan, III, W. T. and Kerstholt, J. H. (1976). *Fluxes and circular polarization of 18 CM OH features over the period 1965-1972*, A&A **26**: 399-403.

Szymczak, M., Gérard, E. (2009). *Polarimetric survey of main-line OH masers in star-forming regions*, A&A, **494**: 117.

Tige, J., Motte, F., Russeil, D., Zavagno, A., Hennemann, M., Schneider, N., Hill, T., Nguyen Luong, Q., di, Francesco J., Bontemps, S., Louvet, F., Didelon, P., Konyves, V., Andre, P., Leuleu, G., Bardagi, J., Anderson, L. D., Arzoumanian, D., Benedettini, M., Bernard, J. -P., Elia, D., Figueira, M., Kirk, J., Martin, P. G., Minier, V., Molinari, S., Nony, T., Persi, P., Pezzuto, S., Polychroni, D., Rayner, T., Rivera-Ingraham, A., Roussel, H., Rygl, K., Spinoglio, L., White, G. J. (2017). *VizieR Online Data Catalog: HOBYS: 46 MDCs found in NGC 6334 (Tige+, 2017)*, A&A, **602**: 77

Townes, C. H., Gordon, J. P., Zeiger, H. J. (1954). *Molecular Microwave Oscillator and New Hyperfine Structure in the Microwave Spectrum of NH₃*. Physical Review, **95**: 282.

Turner, B. E. (1970). *Anomalous Emission from Interstellar Hydroxyl and Water (concluded)*, jrasc, **64**: 282.

Turner, B. E. (1970). *Masers in Space*, pasp, **82**:996.

Weaver, H., Dieter, N. H., Williams, D. R. W. (1968). *Observations of OH Emission in W3, NGC 6334, W49, W51, W75, and ORI*, ApJS, **16**: 219.

Weaver, H., Williams, D. R. W., Dieter, N. H., Lum, W. T. (1965). *Observations of a Strong Unidentified Microwave Line and of Emission from the OH Molecule*, Nature, **208**: 29.

Weinreb, S., Meeks, M. L., Carter, J. C. (1965). *Observations of Polarized OH Emission*, Nature, **208**: 440.

Willis, S., Marengo, M., Allen, L., Fazio, G. G., Smith, H. A., Carey, S. (2013). *A Wide-field near- and Mid-infrared Census of Young Stars in NGC 6334*, Apj Wilson, C. D., Walker, C. E., Thornly, M. D., (1997). *The Density and Temperature of Molecular Clouds in M33*, astro-ph, **1**: 1-33.

- Wilson, W. J. Barrett, A. H. (1968). *Discovery of Hydroxyl Radio Emission from Infrared Stars*, *Science*, **161**: 778-779.
- Wilson, T. L., Walmsley, C. M., Jewell, P. R., Snyder, L. E. (1984). *Detection of a new type of methanol maser*, *A&A*, **134**, L7.
- Winnberg, A., Graham, D., Walmsley, C. M., Booth, R. S. (1981). *A new 1720 MHz OH outburst in V1057 Cyg*, *A&A*, **93**: 79-84.
- Wright, M. (2001). *Probing the star forming region W3(OH) with ground state hydroxyl maser*. University of Bristol, PhD Thesis.
- Wynn-Williams, C. G. and Becklin, E. E., Neugebauer, G. (1972). *Discovery of New Infrared Sources Associated with W3*, **4**: 232.
- Zinnecker, H., Yorke, H. W. (2007). *Toward Understanding Massive Star Formation*, *ARA&A*, **45**: 481.